The challenges of an in situ validation of a non-equilibrium model of soil heat and moisture dynamics during fires

William J. Massman[1]

[1]USDA Forest Service, Rocky Mountain Research Station, 240 West Prospect Road, Fort Collins, CO 80526 USA

Correspondence: W. J. Massman (william.j.massman@usda.gov)

Abstract. With the increasing frequency and severity of fire there is an increasing desire to better manage fuels and minimize, as much as possible, the impacts of fire on soils and other natural resources. Piling and/or burning slash is one method of managing fuels and reducing the risk and consequences of wildfire, but the repercussions to the soil, although very localized, can be significant and often irreversible. In an effort to provide a tool to better understand the impact of fire on soils, this study outlines

5   the improvements to and the in-situ validation of a non-equilibrium model for simulating the coupled interactions and transport of heat, moisture and water vapor during fires. Improvements to the model eliminate two important (but heretofore universally overlooked) inconsistencies: one that describes the relationship between evaporation and condensation in the parameterization of the non-equilibrium vapor source term and the other, is the incorrect use of the apparent thermal conductivity in the soil heat flow equation. The first of these enhanced the stability and performance of the model. The second is an important improvement

10   in the model's physical realism, but had less of an impact on the model's performance and stability than the first. The model validation uses (in-situ temperature, soil moisture, and heat flux) data obtained in a 2004 experimental slash pile burn. Important temperature dependent corrections to the instruments used for measuring soil heat flux and moisture are also discussed and assessed. Despite any possible ambiguities in the calibration the sensors or the simplicity of the parameterization of the surface heating function, the difficulties and complexities of formulating the upper boundary condition, and the obvious complexities

15   of the dynamic response of the soil's temperature and heat flux, the model produced at least a very credible, if not surprisingly good, simulation of the observed data. This study then continues with a discussion and sensitivity analysis of some important feedbacks (some of which are well known and others that are more hypothetical) that are not included in the present (or any extant) model, but undoubtedly are dynamically influencing the physical properties of the soil in-situ during the fire and thereby modulating the behavior of the soil temperature and moisture. This manuscript concludes with a list of possible future

20   observational and modeling studies and how they would advance the research and findings discussed here.

1 Introduction

Fire has been a largely beneficial part of the landscape in most areas of the world for millenia (Harrison et al. , 2010). But,

25   over the past few decades fire has increased significantly in frequency, extent and severity to the point that it now poses substantial risks to most of the world's wildlands and forested ecosystems and the goods and services they provide (e.g., Kasischke and Turetsky (2006); Mortiz et al. (2012); Abatzogloua and Williams (2016); Stambaugh et al. (2018); San-Miguel-Ayanz et al. (2019)). Consequently, there is an increased desire to reduce wildfire risk by better management of fuels, to mitigate the consequences of fire by improving management methods and to promote the recovery of soils and vegetation

30   after fire (e.g., Millar et al. (2007); McCaffrey et al. (2015); Vallejo and Alloza (2015); Schoennagel et al. (2017); Dey and Schweitzer (2018)). Unfortunately for soils, managing fuels often takes the form of biomass burning (i.e., prescribed burns), the consequences of which for the affected area can be as bad as or even worse than wildfire. Therefore, to achieve any of these desired outcomes for managing the ecological effects of fire it is necessary to improve our understanding of the impacts that fire and extreme heating can have on soils. An important and extremely useful tool in this effort is better models of soil

35   heating during fires. Here I summarize the changes made to the HMV-Model (Massman , 2015) and assess the improvements they made to the model's performance by comparing modeled and observed (in situ) soil temperatures, heat fluxes and changes soil moisture during an slash pile burn (Massman et al. , 2008).

The HMV-model is a 1-d (soil depth) model with three time-dependent predictive variables: temperature $= T_K$ (K) or T (C), soil water potential $= \psi$ (Jkg^{-1}) (where $\psi < 0$ and is relatable to volumetric soil moisture θ (m^{3}m^{-3}) through a water

40   retention curve), and soil vapor $= \rho_v$ (kgm^{-3}). At any specific depth, the model assumes thermal equilibrium between the soil matrix, the soil vapor, and the soil moisture. However, it is termed a 'non-equilibrium' model because it does not assume a priori that the soil moisture and soil vapor are in equilibrium, contrary to the equilibrium approach that has been the basis of virtually all models of coupled heat and moisture flow in soils since Philip and de Vries (1957) and de Vries (1958). Although the equilibrium assumption has led to many insights into the nature of soil heat and moisture transport processes in

45   the last six decades, it must fail at some point as the soil dries out for the simple reason that it is difficult to maintain vapor in equilibrium with soil moisture when there is little to no soil moisture (Novak (2012); Massman (2015)). In the case of rapid soil heating and drying during fires (Massman , 2015) further indicates that at the drying front, where local soil evaporation rates are highest, θ and ρ_v are forced out of equilibrium as soil moisture rapidly decreases and the soil vapor rapidly increases. Novak (2019) also demonstrates (under less extreme conditions than during fires) that the greatest departure from equilibrium

50   occurs at the drying front. The equilibrium model cannot capture this evaporative disequilibrium, which may explain why soil evaporation is better modeled with a non-equilibrium approach (Smits et al. (2011); Ouedraogo et al. (2013); Massman (2015); Borujerdi et al. (2019)). In fact, the most important change/improvement in the HMV-model (detailed in the next section) is in the parameterization of the vapor source term $= S_v$ (kgm^{-3}s^{-1}), which is the essence of the non-equilibrium approach and its ability to capture the evaporative disequilibrium. As with its predecessor (Massman , 2015), the present vapor

55   source term is formulated on the basis of the Hertz-Knudsen Equation, which Trautz et al. (2015) have suggested better describes evaporation than other non-equilibrium models of S_v. Nonetheless, all extant models of S_v have overlooked (and

therefore include) an implicit and incorrect assumption about soil evaporation that is addressed and corrected in the present study.

The following section also discusses other changes to the HMV-model, including: (a) eliminating the use of the apparent soil thermal conductivity in the soil heat flow equation (also further discussed and justified in the Appendix) and (b) improving the parameterization of the surface energy balance and the upper (soil surface) boundary condition (including the development of a generic soil heating function for use with prescribed burns or wildfires). In addition, this study also discusses the subtleties and difficulties of formulating a universal surface energy balance for soil heating by fire. The third section reviews the site, soils and data of the experimental slash pile burn and the fourth section compares the observations with the model simulations and explores some of the consequences (to the simulations) of some dynamic feedbacks and interactions between the fire and soil physical properties. The fifth section discusses possible future directions for modeling and observational studies. The final section summarizes this study.

2 Model Description

Similar to version 1 of the HMV-model (Massman , 2015), the present version employs a linearized Crank-Nicolson finite difference scheme and was coded and run using MatLab version 2017b. This manuscript also uses the same notation and the same functional parameterizations for the supporting thermodynamic and physical variables as Massman (2015). For this study details concerning these functional parameterizations will be summarized as necessary for clarity and to update with new information or data. Otherwise many details covered by Massman (2015) will not be repeated here. The remainder of this section discusses the physical fundamentals of the changes made to the HMV-model.

2.1 Conservation of Mass and Energy

The HMV-Model is composed of the three conservation equations: the conservation of energy (or maybe more properly the conservation of enthalpy), the conservation of soil liquid water and the conservation of soil water vapor. The conservation of energy is

$$C_s \frac{\partial T}{\partial t} - \frac{\partial}{\partial z}\left[\lambda_s \frac{\partial T}{\partial z}\right] = -L_v S_v + W S_w \equiv -L_v^* S_v \tag{1}$$

where C_s ($\mathrm{Jm^{-3}K^{-1}}$) is the volumetric specific heat of the soil, such that $C_s = C_s(T, \theta)$ is a function of both temperature and volumetric soil moisture; t (s) is time; z (m) is soil depth; λ_s ($\mathrm{Wm^{-1}K^{-1}}$) is soil thermal conductivity, such that $\lambda_s = \lambda_s(T, \theta, \rho_v)$; $L_v = L_v(T_K)$ ($\mathrm{Jkg^{-1}}$) is the enthalpy of vaporization and $-L_v S_v$ represents the change in enthalpy associated with evaporation/condensation; $S_v = S_v(T_K, \theta, \psi, \rho_v)$ is the source term for water vapor and is discussed in more detail in the following section; and $W S_w$ is the change in enthalpy associated with the heat of wetting (also termed the heat of immersion), where W ($\mathrm{Jkg^{-1}}$) is the heat of wetting and S_w ($\mathrm{kgm^{-3}s^{-1}}$) is the source term for water liquid or equivalently the sink term for water vapor, i.e., $S_w \equiv -S_v$. W is discussed by de Vries (1958) and for the present purposes W can be interpreted as

that additional enthalpy of vaporization that is required to break the electrostatic bonds between molecular water and the soil mineral surfaces. In general the wetting reaction is exothermic, i.e., $W > 0$ and a function of temperature (Grant (2003); Prunty and Bell (2005)). Massman (2012) investigated the effects of temperature on ψ and W, but found that it had little

90   impact on the modeling results. For this study the HMV-model follows Campbell et al. (1995) and assumes that $W = -\psi$ and ignores any temperature dependencies of ψ and W. Note that W is only significant at high temperatures (as $L_v \to 0$) and for extremely dry soil (as $-\psi \to \infty$). Finally with this identification for W and the above identity between S_w and S_v, it follows that $L_v^* \equiv L_v - \psi$.

The conservation of liquid water is

95    $$\rho_w \frac{\partial \theta}{\partial t} - \rho_w \frac{\partial}{\partial z}\left[K_n \frac{\partial \psi_n}{\partial z} + K_H - V_{\theta,surf}\right] = -S_v \qquad (2)$$

where $\rho_w = \rho_w(T_K)$ (kgm^{-3}) is the density of liquid water; ψ_n (dimensionless) is the non-dimensional form of ψ, i.e., $\psi_n = \psi/\psi_*$, where $\psi_* = -10^6$ Jkg^{-1} is the nominal soil water potential of oven-dried soil ((Campbell et al. , 1995)). (Note ψ_n is used interchangeably with ψ throughout this manuscript.) $K_n = K_n(T_K, \psi_n, \theta)$ (m^{2}s^{-1}) is the hydraulic diffusivity; $K_H = K_H(T_K, \psi_n, \theta)$ (ms^{-1}) is the hydraulic conductivity; and $V_{\theta,surf} = V_{\theta,surf}(T_K, \theta)$ (ms^{-1}) is the velocity of liquid

100   water associated with surface diffusion of water. The hydraulic conductivity functions, $K_n(T_K, \psi_n, \theta)$ and $K_H(T_K, \psi_n, \theta)$, are given as follows:

$$K_n = \frac{K_I K_R \rho_w}{\mu_w}\psi_* \qquad \text{and} \qquad K_H = \frac{K_I K_R \rho_w}{\mu_w}g \qquad (3)$$

where $\mu_w = \mu_w(T_K)$ (Pas) is the viscosity of water; $g = 9.81$ ms^{-2} is the acceleration due to gravity; K_I (m^2) is the intrinsic permeability of the soil here assumed to be constant and uniform throughout the soil profile, but does, in fact, vary with the

105   concentration and type of solutes in soil water, (e.g., Lutz and Kemper , 1959); and $K_R = K_R(\theta, \psi_n, T_K)$ (dimensionless) is the relative hydraulic conductivity (used to describe capillary flow in soils). The model for intrinsic permeability is taken from Bear (1972) and is $K_I = (6.17 \times 10^{-4})d_g^2$; where d_g (m) is the mean or 'effective' soil particle diameter. Note that switching variables from $\psi < 0$, to ψ_n produces $\psi_n > 0$ and $K_n < 0$. The present model considers only capillary flow and will ignore film flow, because like Massman (2015) film flow did not really impact the model's performance.

110   The conservation of water vapor is

$$\frac{\partial(\eta - \theta)\rho_v}{\partial t} - \frac{\partial}{\partial z}\left[D_{ve}\frac{\partial \rho_v}{\partial z} - (\eta - \theta)u_{vl}\rho_v\right] = S_v \qquad (4)$$

where η (m^{3}m^{-3}) is the total soil porosity, assumed to be temporally constant and spatially uniform, and $(\eta - \theta)$ is the soil's air filled porosity; and $D_{ve} = D_{ve}(T_K, \psi, \rho_v)$ (m^{2}s^{-1}) is the (equivalent) molecular diffusivity associated with the diffusive transport of water vapor in the soil's air-filled pore space, where D_{ve} includes the enhancement factor developed by Campbell

115 et al. (1995) and detailed in Massman (2012); and u_{vl} (ms^{-1}) is the advective velocity induced by the change in volume associated with the rapid volitalization of soil moisture, which is given as follows:

$$\frac{\partial u_{vl}}{\partial z} = \frac{S_v}{(\eta - \theta)\rho_v} \qquad (5)$$

The final model equations result by preserving Equation (4) and eliminating S_v from Equations (1) and (2), such that Equation (1) is replaced with

120
$$C_s \frac{\partial T}{\partial t} - \frac{\partial}{\partial z}\left[\lambda_s \frac{\partial T}{\partial z}\right] - L_v^* \rho_w \left(\frac{\partial \theta}{\partial t} - \frac{\partial}{\partial z}\left[K_n \frac{\partial \psi_n}{\partial z} + K_H - V_{\theta,surf}\right]\right) = 0 \qquad (6)$$

and Equation (2) is replaced with

$$\rho_w \frac{\partial \theta}{\partial t} - \rho_w \frac{\partial}{\partial z}\left[K_n \frac{\partial \psi_n}{\partial z} + K_H - V_{\theta,surf}\right] + \frac{\partial(\eta - \theta)\rho_v}{\partial t} + \frac{\partial}{\partial z}\left[D_{ve}\frac{\partial \rho_v}{\partial z} - (\eta - \theta)u_{vl}\rho_v\right] = 0 \qquad (7)$$

2.2 Improvements in Non-equilibrium Vapor Source Term

Massman (2015, Equation(10)) adapted the Hertz-Knudsen Equation to develop the following formulation for the vapor source
125 term, S_v,

$$S_v = S_* A_{wa} \sqrt{\frac{RT_K}{M_w}}\left(\mathcal{K}_e \rho_{v,eq} - \mathcal{K}_c \rho_v\right) \qquad (8)$$

where S_* is an empirical dimensionless parameter, which is "tuned" as necessary to ensure model stability; A_{wa} (m^{2}m^{-3} or m^{-1}) is the volume-normalized soil water-air interfacial surface area, which Massman (2015) parameterized as $A_{wa} = A_{wa}(\theta)$; $R = 8.314$ Jmol^{-1}K^{-1} is the universal gas constant; $M_w = 0.01802$ kgmol^{-1} is the molar mass of water vapor; $\mathcal{K}_e$
130 (dimensionless) is the mass accommodation (or evaporation) coefficient, which Massman (2015) sets $\equiv 1$; $\mathcal{K}_c = \mathcal{K}_c(T_K, \psi_n)$ (dimensionless) is the thermal accommodation (or condensation) coefficient, which Massman (2015) parameterizes as a physicochemical (Arrhenius) function: $\mathcal{K}_c(T_K, \psi_n) = e^{\frac{E_{av} - M_w\psi}{R}\left(\frac{1}{T_K} - \frac{1}{T_{K,in}}\right)}$, where $E_{av} - M_w\psi$ (Jmol^{-1}) is an empirical surface condensation/evaporation activation energy for which $E_{av} \approx 30 - 40$ kJmol^{-1} was determined empirically and $T_{K,in}$ is the initial soil temperature; and $\rho_{v,eq}$ (kgm^{-3}) is the equilibrium vapor density, defined as $\rho_{v,eq} = a_w\rho_{v,sat}(T_K)$ where
135 $a_w = e^{\frac{M_w\psi_*}{RT_K}\psi_n}$ is the dimensionless water activity, modeled here with the Kelvin Equation, and $\rho_{v,sat}(T_K)$ (kgm^{-3}) is the saturated vapor density, which is a function only of T_K.

But the model of S_v embodied by Equation (8) assumes that the interfacial surfaces appropriate to evaporation and condensation are the same, i.e., that A_{wa} is the same for both evaporation $\left(\sqrt{RT_K/M_w}\mathcal{K}_e\rho_{v,eq}\right)$ and condensation $\left(\sqrt{RT_K/M_w}\mathcal{K}_c\rho_v\right)$. In general this is not a priori the case unless one assumes that soil moisture (θ) never drops below the point at which the soil's in-
140 terfacial surface area is completely covered by a thin film or mono-layer of liquid water (e.g., Novak , 2019). But it is physically

more realistic, at least for very dry soils (which are likely to occur during fires), to assume that condensation can occur even in the absence of liquid water. Otherwise models of S_v would impose a physically unrealistic constraint on non-equilibrium models of heat and moisture flow in dry soils.

The new version of the non-equilibrium model parameterizes S_v as follows:

$$S_v = S_* \sqrt{\frac{RT_K}{M_w}} \left(A_{wa}(\theta) \rho_{v,eq} - A_{wa,dry} \mathcal{K}_c \rho_v \right) \tag{9}$$

where $\mathcal{K}_e \equiv 1$ has been retained as has the original formulation for A_{wa} (Massman , 2015):

$$A_{wa}(\theta) = \mathcal{S}_w (1 - \mathcal{S}_w)^{a_1} + a_2 [\mathcal{S}_w (1 - \mathcal{S}_w)]^{a_3} \tag{10}$$

where $\mathcal{S}_w = \theta/\eta$ is the soil water saturation and $a_1 = 50$ (rather than the original value of 40), $a_2 = 0.003$, and $a_3 = 1/8$. This particular value for the parameter a_1 was chosen so that the maximum value of A_{wa} occurs at $\mathcal{S}_w \approx 0.02 (= 1/a_1)$, and is assumed to be where the soil surfaces are covered by a mono-layer of water (Brusseau et al, , 2006). $A_{wa,dry} \equiv A_{wa}(\theta)$ as long as $\mathcal{S}_w > 1/a_1$, and $A_{wa,dry} \equiv \max(A_{wa})$ whenever $\mathcal{S}_w \leq 1/a_1$. In other words, $A_{wa,dry}$ differs from A_{wa} whenever the soil moisture is so low that the soil particle surfaces are covered by, at most, a mono-layer of water. Empirical "tuning" of S_* and E_{av} after implementing the other changes yielded $S_* = 0.1$ and $E_{av} = 10 \ \mathrm{kJmol}^{-1}$. Together these changes to S_v improved the model's stability and robustness, as well as, it's fidelity to the observed soil moisture during the 2004 burn (detailed later).

2.3 Corrections and Improvements in Soil Thermal Conductivity

The present model of λ_s retains (a) the general structure of the original Campbell-de Vries model for thermal conductivity (see Campbell et al. (1994), de Vries (1963) and Massman (2012)) and (b) the additional Bauer term associated with the high-temperature thermal (infrared) radiant energy transfer within the soil pore space (Bauer , 1993). That is

$$\lambda_s = \frac{k_w \theta \lambda_w(T_K, \rho_w) + k_a [\eta - \theta] \lambda_a^*(\theta, T_K, \rho_v) + k_m [1 - \eta] \lambda_m}{k_w \theta + k_a [\eta - \theta] + k_m [1 - \eta]} + 3.8 \sigma N^2 R_p T_K^3 \tag{11}$$

where k_w, k_a, and k_m (dimensionless) are the Campbell et al. (1994) generalized formulations of the de Vries (1963) weighting factors; $\lambda_w(T_K, \rho_w)$ $(\mathrm{Wm}^{-1}\mathrm{K}^{-1})$ is the thermal conductivity of liquid water; $\lambda_a^*(\theta, T_K, \rho_v)$ $(\mathrm{Wm}^{-1}\mathrm{K}^{-1})$ is the apparent thermal conductivity of moist air, which is the sum of the true thermal conductivity of moist air, $\lambda_a(\theta, T_K, \rho_v)$ $(\mathrm{Wm}^{-1}\mathrm{K}^{-1})$ and the term, $\lambda_v^*(\theta, T_K, \rho_v)$ $(\mathrm{Wm}^{-1}\mathrm{K}^{-1})$, which embodies the effects of latent heat transfer or "the effect of the vapor distillation due to temperature gradients" (de Vries (1958); Appendix A of the present study); λ_m $(\mathrm{Wm}^{-1}\mathrm{K}^{-1})$ is the thermal conductivity of the mineral components of the soil; σ $(\mathrm{Wm}^{-2}\mathrm{K}^{-4})$ is the Stefan-Boltzmann constant; $N = N(\theta) = 1 + \theta/(3\eta)$ (dimensionless) is the pore gas index of refraction; and R_p (m) is the soil's pore space volumetric radius. The first term on the right hand side of Equation (11) is the Campbell-de Vries model and the second is the Bauer term.

The weighting factors, k_w, k_a, and k_m all have the same general form (Campbell et al. , 1994):

$$k_* = k_*(\theta, T) = \frac{1}{3}\left[\frac{2}{1 + (\frac{\lambda_*}{\lambda_f} - 1)g_a} + \frac{1}{1 + (\frac{\lambda_*}{\lambda_f} - 1)(1 - 2g_a)}\right] \tag{12}$$

170 where the subscript $*$ refers to water (w), air (a), or mineral (m); g_a is the de Vries (1963) shape factor, an empirically determined model parameter. In general $g_a \approx 0.1$ (Campbell et al. , 1994). $\lambda_f = \lambda_f(\theta, T)$ is a weighted mixture of the thermal conductivities of air and water:

$$\lambda_f(\theta, T) = \lambda_a(\theta, T, \rho_v) + f_w(\theta, T)[\lambda_w(T) - \lambda_a(\theta, T, \rho_v)] \tag{13}$$

and

175 $$f_w(\theta, T) = \frac{1}{1 + (\frac{\theta}{\theta_w})^{-q_w(T)}} \tag{14}$$

where $q_w(T_K)$ is a dimensionless parameter that describes the water content at which water begins to influence λ_s. It is defined as $q_w(T_K) = q_{w0}(T_K/303)^2$ with q_{w0} another empirically determined parameter. g_a and q_{w0} are important for the present study because they are an important part of the sensitivity analysis (discussed in a later section) that explores the interactions between the fire and the soil physical properties.

180   Three changes have been made to this original formulation. First, λ_v^* is no longer included because to do so is to double count the vapor "distillation" (de Vries , 1958) term that accounts for the influence that evaporation, transport and condensation of water vapor can have on the apparent thermal conductivity (Appendix A). In other words as shown in Appendix A, both equilibrium and non-equilibrium models of soil heating include the vapor distillation term, either explicitly through the conservation of mass of water vapor (non-equilibrium models) or implicitly through the conservation of mass of liquid

185 water (equilibrium models). Consequently, it is unnecessary and redundant to include λ_v^* in Equation (11). Second, λ_m now includes an explicit temperature dependency of the form $\lambda_m = \lambda_m(T_K) = \lambda_{m0}(8\exp(-0.008(T_K - 300)) + 3)/11$; where λ_{m0} (Wm^{-1}K^{-1}) is basically an adjustable parameter. The results for α-quartz (α referring to a specific crystalline structure of quartz) from (Yoon et al. , 2004, Figure 4) suggests that it is reasonable to expect that $\lambda_{m0} \leq 15$ Wm^{-1}K^{-1}. The temperature function $(8\exp(-0.008(T_K - 300)) + 3)/11$ was chosen to emulate the approximately 70% decrease in the thermal conduc-

190 tivity of α-quartz (here used as a substitute for sand quartz) between about 300 K and 600 K shown by Kanamori et al. (1968) and Yoon et al. (2004). Third, R_p is now estimated as $R_p = 0.408d_g\sqrt{(\rho_p/\rho_b) - 1}$ from Arya et al. (1999); where d_g (m) is the mean or "effective" soil particle diameter, ρ_p (Mgm^{-3}) is the particle density (which can usually be assumed to be about 2.65 Mgm^{-3} and ρ_b (Mgm^{-3}) is the soil bulk density. This formulation for R_p yields more physically realistic estimates of R_p (i.e., 5 μm $\leq R_p \leq$ 200 μm for the soils tested in this study) than the default value of 1000 μm used in the previous version

195 of the HMV-model. It also suggests that the thermal infrared contribution to the soil thermal conductivity is negligible in most soils, even during fires.

2.4 Evaluation of changes to S_v and λ_s

Assessing the consequences of these alterations to the source term and soil thermal conductivity to the model's performance was done using the laboratory data of Campbell et al. (1995) and by comparing the simulations with the changes to S_v and

200   λ_s to those shown in Massman (2015). The results indicated that (a) the model's ability to faithfully reproduce the data were very similar to those in Massman (2015) and (b) the model's stability was significantly improved. The reason for (b) is (almost exclusively attributable to) the change in S_v and is very much a positive benefit to the model. The changes to λ_s, did require some adjustments to the values of some of the other parameters included in the model for λ_s, but these were minimal and not particularly significant. For the sake of brevity, none of these comparisons are included in this study.

205 ## 2.5   Complexities and Challenges

2.5.1   Surface Heating, Surface Energy Balance and Upper Boundary Condition

The forcing function is the energy that is input to the soil at its surface, denoted here by $Q_F(t)$ (Wm^{-2}). How that energy is divided between net infrared heat loss, convective heat loss, evaporation, and soil conductive heating is expressed by the surface energy balance and the upper boundary conditions. Although relatively simple in concept, in practice, for application

210   to fires the forcing function, the surface energy balance and the upper boundary all are at best difficult to formulate precisely and at worst potentially a fiction. For example, in the case of a wildfire or soil heating within a few meters outside the physical perimeter of a slash pile surface forcing is primarily radiant energy. See Fig.2 of Massman et al. (2010a) for an example of this second case. On the other hand, when burning material makes direct contact with the soil, it is reasonable to assume that the forcing at the soil surface is more likely to be conduction rather than radiant energy. Beneath a slash pile burn surface forcing

215   may be combination of radiation and conduction, it may change over time as the pile burns, as the ash accumulates and, at later stages of the burn, as the pile collapses. In the case of a moving fire front, the forcing can be highly variable. Radiant energy is clearly a major driver, but in addition, thermal instabilities drive circulations ahead and behind the fire that input energy into the soil when these circulations force hot air into contact with the soil, which in turn causes direct ignition of soil biomass ahead of the flame front (Finney et al. , 2015; Pearce et al. , 2019; Linn , 2019). As the fire front passes the forcing

220   is likely to be a combination of conduction and radiation and possibly convection. Whereas after the fire front conduction is the major forcing in areas covered with burning biomass, and radiant energy and possibly convection in areas free of burning biomass. Finally, in the case of burning duff, forcing is likely to be solely conductive in nature; but complications arise because in this situation duff is a highly porous burning insulator. Parameterizing the forcing in this case is problematic because of the extremely limited (empirical and theoretical) knowledge concerning burning duff.

225   Massman (2015) assessed the performance of the previous version of the HMV-model against the laboratory data of Campbell et al. (1995), which more or less dictated the following forcing function: $Q_F(t) = Q_{Fmax}(1 - \exp(-t/\tau))$; where τ (s) and Q_{Fmax} (Wm^{-2}) are adjustable parameters that describe the rate of rise of the forcing function (τ) and its stead state

asymptotic (maximal) value Q_{Fmax}. This study uses the following modified form of the BFD curve (Barnett , 2002) as the forcing function

230
$$Q_F(t) = Q_{Fin} + (Q_{Fmax} - Q_{Fin})e^{-\alpha(\ln(t/t_m))^2} \tag{15}$$

where $e^{-\alpha(\ln(t/t_m))^2}$ is the modified BFD-curve; t_m (s) is the time at which the maximum forcing occurs, and α (dimensionless) $= 2\ln(10)/(\sinh^{-1}[0.5t_d/t_m])$ and t_d (s) is the time interval between when the forcing first reaches 1% of its maximum and when it has decayed to 1% of its maximum. Q_{Fmax}, t_m and t_d are adjustable input parameters to the model that define the forcing function, much the same way that Q_{Fmax} and τ are for the Campbell et al. (1995) forcing function. Q_{Fin} (Wm^{-2}),

235 on the other hand, is not an adjustable input parameter. It is determined from other considerations of the soil surface energy balance and is define later. The boundary conditions for temperature and vapor pressure, e_v (Pa), have similar functional forms as Equation (15): $V_a = V_{in} + V_{max}e^{-\alpha(\ln(t/t_m))^2}$; where V_a refers to the ambient atmospheric temperature (T_a) or vapor pressure ($\rho_{v,a}$) at the soil surface and the subscript 'in' refers to the initial value of that variable (taken from observations near the time and location of the fire). V_{max} is an adjustable model input parameter 'tuned' so that the model matches (as much as

240 possible) the soil observational data and (if necessary) to help ensure model stability. The vapor density boundary condition is derived from these latter two boundary conditions using the ideal gas law. The upper boundary condition on soil moisture is $(\partial\theta/\partial z)_0 = 0$ and is discussed further in Massman (2015).

The energy balance at the soil surface used with the present study is slightly different from either Massman (2012) or Massman (2015). Here it is expressed as

245
$$\epsilon_0(\theta_0)Q_F(t) = \epsilon_0(\theta_0)\sigma\left[T_{K0}^4 - \epsilon_a(\rho_{va})T_{Ka}^4\right] + \rho_a c_{pa} C_H\left[T_0 - T_a\right] + L_{v0}^* E_0 + G_0 \tag{16}$$

where the '0' subscript refers to soil surface and the term on the left hand side of this equation is the energy absorbed by the soil (and assumes that absorptivity and emissivity of the soil are the same) and the first term on the right hand side is the net infrared heat loss, the second is the convective heat loss, the third is rate of evaporation, and the last is the soil conductive heat; $\epsilon_0(\theta_0)$ is the soil emissivity and is a function of the soil moisture, θ_0; $\sigma = 5.67 \times 10^{-8}$ Wm^{-2}K^{-4} is the Stefan-Boltzmann

250 constant; $\epsilon_a(\rho_{va})$ is the emissivity of the ambient atmosphere exposed to the soil surface during the fire and is a function of the ambient vapor density ρ_{va} following the 'clear sky' parameterization of Brutsaert (1984, Equation (6.18)); $\rho_a = \rho_a(T_{K0}) = 1.29(P_a/P_{ST})(T_{ST}/T_{K0})$ (kgm^{-3}) is the mass density of the ambient air at the soil surface temperature, T_{K0}, where P_a (Pa) is the ambient pressure (at the time and location of the fire and is a model input variable) and $P_{ST} = 101325$ Pa and $T_{ST} = 273.15$ K are the standard atmospheric pressure and temperature; $C_H = 0.032$ (ms^{-1}) is the transfer coefficient for

255 convective heat from the surface (see Massman (2012) or Massman (2015)). $T_a = T_a(t)$ (C), or equivalently $T_{Ka} = T_{Ka}(t)$ (K), is the ambient temperature somewhere above the soil surface (upper boundary condition); $L_{v0}^* E_0$ (Wm^{-2}) is the rate of soil water evaporation; E_0 (kgm^{-2}s^{-1}) is the evaporative mass flux at the surface; and G_0 (Wm^{-2}) is the soil conductive heat

flux and the upper boundary condition for the modeled soil temperatures, Equation (6). E_0 is parameterized as the sum of a diffusional component and an advective component (Massman , 2012):

260
$$E_0 = C_E h_{s0} \left[\rho_{v0} - \rho_{va}(t) \right] + C_U u_{vl0} \rho_{v0} \qquad (17)$$

where C_E (ms^{-1}) and C_U (dimensionless) are adjustable model transfer coefficients, which were determined empirically to maximize E_0 without destabilizing the model. $C_U = 0.125$ is associated with the jet of volitalized air emanating from the soil with velocity u_{vl0} and $C_E = 10^{-4}$ ms^{-1}. The surface humidity, h_{s0} (dimensionless), is assumed to be the same as a_{w0}, the water activity at the surface.

265   Although Equation (16) provides a complete accounting of the energy exchange between the atmosphere and the soil, there are two key issues that need to be addressed when initializing the model for applications to fires. The first was mentioned earlier, i.e., under a burning slash pile or a soil covered (partially or completely) with an ash layer it is not clear what the infrared and convective heat environments really are or what role they may play in the soil energy balance. This issue is relevant here because the data used in this study was obtained under a burning slash pile and it is addressed in the present study in a later

270   section on sensitivity analysis by comparing model simulations with and without the IR and convective heat terms. Removing these later two terms from Equation (16) yields the following simplified version of the soil surface energy balance:

$$\epsilon_0(\theta_0) Q_F(t) = L_{v0}^* E_0 + G_0 \qquad (18)$$

The second issue is basically a feature of all forcing functions. In the case of the BFD-curve, $t_m \geq 0.5$ hr is always true and because a typical model time step is between 1 and 4 s, there will always an initial period between a few minutes to

275   several tens of minutes long where the simulated burning time $t \ll t_m$. During this "ramp-up" period $Q_F \approx Q_{Fin}$. The choice of Q_{Fin} depends on whether Equation (16) or Equation (18) is used. In the case of Equation (18), $Q_{Fin} = 0$. In this case the soil conductive heat flux becomes $G_0 = -L_{v0}^* E_0$, and because the source term and the evaporation rates are very nearly at equilibrium (i.e., $S_v \approx 0$ and $E_0 \approx 0$) during this ramp-up, it follows that $G_0 \approx 0$ and that $\partial T / \partial t \approx 0$. (Note: the soil is initialized to be isothermal at the temperature obtained at the soil surface just before initiating the burn.) But for Equation (16),

280   the full surface energy balance equation, this equilibrium condition does not occur during the ramp-up if $Q_{Fin} = 0$, because the net IR term in Equation (16) is not initially in equilibrium. This is true despite initializing $T_a = T_0$. Without Q_{Fin} Equation (16) reduces to $G_0 \approx -\epsilon_0(\theta_0)\sigma T_{K0}^4(1 - \epsilon_a(\rho_{va})) < 0$, which induces a transient in the solution that causes the soil temperature to drop slightly (i.e., $\partial T / \partial t < 0$). But assigning $Q_{Fin} \approx \sigma T_{K0}^4(1 - \epsilon_a(\rho_{va}))$ eliminates this transient and ensures that $G_0 \approx 0$ and $\partial T / \partial t \approx 0$ during the ramp-up time. Several other methods were tested for eliminating this unrealistic solution, but the present

285   approach proved to be the least intrusive and best way to prevent this initial transient. Note: this initial period of disequilibrium in the surface energy balance is not unique to the modified BFD curve. It also occurred with other forcing functions that were tested (e.g., Blagojević and Pešić , 2011) as well as with the Campbell forcing function used in Massman (2012) and Massman (2015).

2.5.2 The Lower Boundary Condition and Initial Conditions

290 The lower boundary condition is the same "pass through" or "extrapolative" boundary condition that was used in Massman (2012) and Massman (2015), i.e., the second derivative, $\partial^2/\partial z^2$, of the 3 model variables = 0. But for the present study (which is devoted to wildfires and slash pile burns, rather than the laboratory experiments of Campbell et al. (1995)), the lower boundary is placed at 0.60 m below the surface (well below 0.20 m used in these previous studies). This pass through boundary condition is used because for field-based applications the lower boundary condition will never be known (or knowable

295 without extraordinary effort before hand) so it must be fairly general and placed at a depth where it will not influence the model predictions within the upper few centimeters of soil too much. The advective velocity, u_{vl}, requires only one boundary condition, see Equation (5), and is $u_{vl} = 0$ at the bottom boundary.

The initial conditions for soil temperature and moisture are taken from measurements made just before igniting slash pile. The soil temperature is assumed to be uniform throughout the vertical domain and is taken to be the observed soil surface

300 temperature. The initial soil vapor pressure is estimated to be about 40% of the saturation vapor pressure at the initial soil temperature. The ideal gas law is then used to estimate the initial soil vapor density profile. The initial soil water potential is obtained from the soil moisture data using the water retention curve, discussed next.

2.6 The Water Retention Curve

Unlike the previous studies (Massman (2012), Massman (2015)), which employed soils for which the water retention curve

305 was unavailable, the present study does employ a water retention curve appropriate to the soils at the site of the experimental burn (Manitou Experimental Forest: MEF). Figure 1 shows the WRCs for pre-burn (red) and post-burn (black) soils the MEF burn site. Note: both pre- and post-burn soils are included in this study because they are part of the model sensitivity analysis. The data shown in this figure were provided by Butters (2009) and were obtained from a 2008 burn study performed at a site about 60 m away from the 2004 burn discussed in this study. The data were fit with the Fredlund and Xing (1994) model:

310 $$\theta/\eta = \mathcal{S}_w = \left(1 - \frac{\ln(1 + a\psi_n)}{\ln(1 + a)}\right)\left(\ln(e + (b\psi_n)^n)\right)^{-m} \qquad (19)$$

where $a > 0$, $b > 0$, $n > 0$, and $m > 0$ are fitting parameters, e is Euler's Number, and the total porosity η was established beforehand such that $\eta_{pre} \approx 0.51$ and $\eta_{post} \approx 0.45$. These values of η correspond to the following values of soil bulk density: $\rho_{b,pre} = 1.30$ Mgm^{-3} and $\rho_{b,post} = 1.46$ Mgm^{-3}. This change in bulk density is revisited in the model sensitivity analysis. Although the Fredlund-Xing model provided the best fit to the data, other models of the WRC were fit to the observations.

315 For the HMV-model the choice of WRC is important. The Fredlund-Xing model did provide the best fit to the data and its impact on model performance was judged the best of the models tested. Other models for the WRC that were tested include the Campbell-Shiozawa model (Campbell and Shiozawa , 1992), which was used in both Massman (2012) and Massman (2015), the van Genuchten model (van Genuchten , 1980), and the Groenevelt-Grant model (Groenevelt and Grant , 2004). For the purposes of model performance, the key difference between Fredlund-Xing model, Equation (19) and Campbell-Shiozawa

320 model, and (the class of models represented here by) the van Genuchten and the Groenevelt-Grant models is the WRC's
description and mathematical behavior when the soil is extremely or completely dry. Under these conditions Equation (19)
when $\theta \approx 0$ the soil water potential remains bounded, i.e., $\psi \approx -10^6$ Jkg^{-1}. But with the van Genuchten and the Groenevelt-
Grant models a completely dry soil is impossible to achieve because $\theta = 0$ can only occur when $\psi = -\infty$. But in the HMV-
model an unbounded function for the WRC does result in the degradation in model performance, some loss of physical realism
325 in the simulation of soil moisture, and can introduce model instabilities.

On the other hand, using a WRC that remains bounded produces a logical inconsistency when used with the Kelvin Equation
to describe water activity and the equilibrium vapor density. This issue plagued earlier modeling attempts (Massman , 2012,
2015). In the case of Massman (2012), when $\theta = 0$, $\psi = -10^6$ Jkg^{-1} and $\partial\psi/\partial t = 0$. But as long as the temperature keeps
rising, $\partial T/\partial t > 0$, it follows that $\partial\rho_{v,eq}/\partial t > 0$. For the equilibrium model ($\rho_v \equiv \rho_{v,eq}$) this means that when the soil moisture
330 is completely evaporated and the soil is dry, the model autonomously creates water vapor. In the case of Massman (2015),
the same inconsistency produces a source term that does not allow condensation to occur (i.e., $S_v < 0$) on the surface of a soil
particle that is completely dry. It is this issue that lead to the improved parameterization of S_v embodied in Equation (9) of the
present study.

2.7 The Hydraulic Functions

335 The hydraulic functions, K_n and K_H, are both basically determined by K_R, as discussed above (Equation (3)). Like Massman
(2015) the present study employs the Assouline model Assouline (2001) for K_R, except here K_R does not include a residual
soil moisture term. Therefore,

$$K_R(\theta) = \left(1 - \left[1 - \left(\frac{\theta}{\eta}\right)^{\frac{1}{m_k}}\right]^{m_k}\right)^{n_k} \tag{20}$$

where m_k and n_k are parameters ($0 < m_k < 1$, and $n_k > 1$) that are adjusted or tuned to ensure that the present model produces
340 a reasonable and physically realistic simulation of the observed soil moisture dynamics during the fire. Unfortunately, there are
no data available to determine K_R for the soil at the MEF burn site.

3 Manitou Experimental Forest: Burn Site and Instrumentation

Much of the general description of climate and physical characteristics of Manitou Experimental Forest and the burn site have
been published previously (Massman and Frank , 2004; Massman et al. , 2006). Nonetheless, for the present purposes they do
345 bear repeating.

3.1 General Site and Soil Description

The burn experiment is located within MEF (39° 04′ N and 105° 04′ W), a dry montane ponderosa pine (*Pinus ponderosa*)
forest in the central Rocky Mountains about 45 km west of Colorado Springs, CO, USA. MEF has a mean elevation of about

2400 m ASL and an annual mean temperature of about 5 C. The annual precipitation is about 400 mm. Soils within MEF
350 tend to have low available water holding capacity and moderately high permeability. The dominant parent materials of the soils
within MEF are primarily Pikes Peak granite and secondarily weathered red arkostic sandstone.

   The area surrounding the burn site is a large grassy opening that had been created in the surrounding ponderosa pine forest in
2001 when several trees were cut in an effort to reduce the amount of mistletoe in the area. The vegetation within this opening
is predominantly grasses, forbs, and shrubs (including some non-native invasives). At the time of the experiment (fall 2003
355 - spring 2004) this opening was covered primarily by senescent bunchgrasses. The soil within the general area of the burn
pile is a deep (> 1.0 m), fine-loamy, mixed, frigid, Pachic Argiustoll and is typical of soils throughout this experimental area.
Soils within the burn area are Pendant cobbly loam and range between 60-65% sand, 20-25% silt, and 10-15% clay with bulk
densities that usually increase with depth (Massman et al. , 2008) and range between 1.1 and 1.5 $\mathrm{Mgm^{-3}}$. Soil organic material
comprises about 1-2% of the soil by volume. Previous grazing and mechanical harvesting throughout the area has resulted in a
360 moderately disturbed soil.

3.2 The Slash Pile Burn: Description and Instrumentation

The burn site instrumentation was installed in August 2003 at two control plots and two slash plots (under the center and the
edge of the slash pile). Data include soil temperatures, soil moisture, soil heat flux, and soil CO_2 at several soil depths. All
these in situ sensors and their associated connectors and cables were buried several centimeters deep and connected to data
365 loggers (CR23X data logger: Campbell Scientific; Logan, UT, USA) via a 27 m trench that had been back-filled to protect the
data communications from the heat of the fire. The slash pile (located at 3.11439° N and 105.10284° W) was mechanically
constructed in March of 2004 and measured about 42 m in circumference, about 6 m in height, and covered an elliptically
shaped area of about 130 $\mathrm{m^2}$. The fuel loading was estimated to be between 450 and 600 $\mathrm{kgm^{-2}}$. The burn was initiated a few
minutes after 10:00 am MDT on April 26, 2004. Figure 2 shows the burning slash pile shortly after the fire was initiated and the
370 deployment of the data loggers, CO_2 pumps and analyzers, and the supporting infrastructure. Note: although the soil CO_2 data
and the data from the edge of the pile are somewhat peripheral to this study, they are included here because they offer some
important insights into some of the assumptions underlying the present model, as is discussed in a later section. Otherwise the
measured soil temperatures, soil moisture and soil heat fluxes are compared to the model's predictions and thereby assess and
validate the model's performance.

3.2.1 Soil Temperature

Soil temperatures were measured with thermocouples (Omega Engineering; Stamford, CT, USA) and sampled every two
minutes during the fire and for the week following the day the fire was initiated. To insure electrical isolation all thermocouple
junctions were coated with epoxy (Omegabond 101) prior to insertion into the soil. Thermocouples were placed at the soil
surface (0.00 m) and at 0.02, 0.05, 0.10, 0.15, 0.20, and 0.50 m depths. The four uppermost sensors, including the soil surface,
380 were K-type (rated to 704 C), the J-type (rated to 260 C) was used at 0.15 m, and the bottom two depths were T-type (rated to
100 C).

3.3 Soil Heat Flux

The soil heat fluxes were measured at three depths (0.02 m, 010 m, 0.20 m) under the center of the pile with a high-temperature probe (HFT) with an aluma core and an exterior ceramic glaze (Thermonetics Corporation, La Jolla, CA). They were also

385 sampled at the same rate and time as the soil thermocouples. These high temperature HFTs are rated to 775 C and have a nominal sensitivity between 1250 and 1750 $\mathrm{Wm^{-2}mV^{-1}}$. These HFTs were attached to a data logger by a cromel extension wire (Omega Engineering TFCH-020, rated to 260 C).

Because these high temperature HFTs are exposed to such a wide range of temperatures (potentially anywhere between about -10 and 700 C) it is important to account for the effects of temperature on the sensors' thermal conductivity and calibration

390 factors. Details concerning the calibration factor are discussed by Massman and Frank (2004) and need not be repeated here. But the details concerning the thermal conductivity of these HFTs are very relevant here and need highlighting. The thermal conductivity of these HFTs, λ_p $(\mathrm{Wm^{-1}K^{-1}})$, is $\lambda_p = 0.7 + 0.003T$ (where T is degrees Celsius). Knowledge of λ_p is important to correct for the discrepancy between the true soil heat flux, G_{soil} $(\mathrm{Wm^{-2}})$, and the measured soil heat flux, G_m, that results whenever λ_p differs from the soil's thermal conductivity, λ_s, (Philip , 1961; Sauer et al. , 2003; Tong et al. , 2019). This

395 relationship, known as Philip's correction, is given as

$$G_{soil} = [1 - \beta r(1 - \epsilon^{-1})]G_m \tag{21}$$

where β is a dimensionless factor related to sensor shape ($\beta = 1.31$ for the square HFTs), r is the sensor's aspect ratio, i.e., the ratio of the sensor's thickness to its horizontal length ($r = 0.19$ for the HFTs), and $\epsilon^{-1} = \lambda_s/\lambda_p$. If a sensor is perfectly matched to its soil environment, then $\lambda_p = \lambda_s$, $G_m = G_{soil}$, and there would be no need to correct for this discrepancy. But,

400 in general, this is unlikely to occur very often at normal daytime or nighttime soil temperatures and so is, therefore, even less likely during a fire. But this correction also requires in situ knowledge of λ_s, which was not (and probably could never have been) measured during the fire. So the model's predicted λ_s is used in Equation (21). As a consequence, the model's predicted G_{soil} will be evaluated against the measured heat flux, G_m, with and without the Philip correction.

3.4 Soil Moisture and CO_2

405 All soil moisture and CO_2 data were measured at 0.05 and 0.15 m depths at both the center and edge position under the slash pile. They were both sampled every half hour for the week during and after the burn. Soil moisture was measured using a specially designed high-temperature TDR (Zostrich Geotechnical; Pullman, WA, USA). The design of this particular probe is fairly standard, but the material used to house the steel needles and the connectors attaching them to the coaxial (data/signal) cables had a much higher melting temperature than normal. Additionally, those external portions of the coaxial cables that

410 were likely to be exposed to high temperatures were wrapped in silicon tape. The calibration factor for this TDR is temperature dependent and is discussed in more detail in the Appendix of Massman et al. (2010a). Like with the soil heat flux, the model's predictions will be evaluated against the TDR measurements with and without the temperature dependent calibration factor.

Soil CO_2 was measured by drawing a continuous sample for approximately 0.5 minutes through 3/8-inch (id) decabond tubing into a LI-820 (LI-COR Inc.; Lincoln, NE, USA) that was housed several m from the slash pile, as shown in Figure 2.

4 Model Performance and Sensitivity Analysis

4.1 Surface Energy Balance

Figures 3 and 4 show the details of the surface energy balance for Equation (16), the model's upper boundary condition that includes the sensible heat and the net infrared terms. Included in Figure 3 is the forcing function, $Q_F(t)$, which shows the shape of the BFD-curve. Figure 5 shows the surface energy balance for Equation (18), which excludes the sensible heat and the net infrared terms. Comparing Figures 4 and 5 suggests that, once tuned appropriately, either formulation of the surface energy balance will give very similar simulations of the evaporative flux, $L_{v0}^* E_0$. Likewise during the period of soil heating (i.e., when $G_0 > 0$), both formulations give similar and reasonable simulations for G_0. But the simplified model of the surface energy balance, Equation (18), does not capture (and in fact cannot capture) G_0 during the period when the soil is cooling (i.e., when $G_0 < 0$, which starts at about 22 hrs in Figures 3 and 4). Without the possibility of radiative and convective cooling of the surface, Equation (18) does not reproduce $G_0 < 0$.

Another important aspect about the surface energy balance that Equation (18) does not capture as well as Equation (16) is the time lag between the maximum in soil heat flux and the maximum in soil temperature. At 0.02 m depth the observed time lag is about 5 hours. Predictions of the time lag with the full surface energy balance, Equation (16), agree almost exactly with observed time lag. But the simplified model predicts a time lag of about 4.6 hrs. This difference in the time lags is not the result of the different choices of t_m, t_d or Q_{Fmax} between the two models of the surface energy balance. Rather Equation (18) inherently constrains the soil heat flux more strongly than Equation (16).

These apparent limitations of the simplified surface energy balance, Equation (18), do not lessen the argument that it may be appropriate for some slash pile burns. Rather these present comparisons suggest that a hybrid of Equations (18) and (16) may be more appropriate. Such a hybrid would employ Equation (18) in the early part of the burn (before significant loss of mass from the slash pile due to combustion) and Equation (16) later after the fire intensity has peaked (i.e., sometime after t_d) when the soil surface or possibly an ash surface is more exposed to the ambient environment.

Other than these two discrepancies the two forms of the surface energy balance give very similar simulations for soil temperature, moisture and other model variables. Nevertheless, because the full surface energy balance provides the more physically realistic simulation it will be used throughout the remainder of this study.

4.2 Soil Temperature

The principal aim of this model is to simulate reasonable and realistic soil temperatures during fires. The comparison between modeled and observed soil temperatures, shown in Figure 6, suggests that the HMV-model with the current set of 'tuned' parameters is reasonably good at this task. Nonetheless, a careful examination of the features of this figure shows some slight

discrepancies in the model's performance: (1) the model does not capture the early temperature rise beginning at about 4 hrs,
445 (2) nor does it capture the secondary maximum temperature at about 20 hrs, (3) it appears to overestimate the maximum 2 cm soil temperatures (at about 21 hrs), and (4) the soil appears to cool off faster than observed (most obvious after about 28 hrs). Discrepancies (1) and (2) are not unexpected because it is impossible for a simple forcing function like the BFD-curve and Equation (15) to produce an exact or even a nearly exact simulation of the observed temperature dynamics during a fire. Any real physical surface forcing will always be far more (dynamically) complex than the BFD-curve, nor could it be easily
450 generalized from one fire to the next. The (relatively significant) overestimation of the 2 cm soil temperatures is not fully understood, but it may be a consequence of mis-measurement of the installation depth of the soil temperature sensors. Half of the (approximately) 60 C over-prediction can be accounted for if the sensor was installed at 2.6 cm rather than 2 cm. It is also possible that λ_s possess greater vertical structure than is included in the model. Finally the issue involving the difference between the observed and modeled rates of cooling, discrepancy (4), seems to be characteristic of all model simulations, not
455 just the simulation shown in Figure 6. Some of this is undoubtedly related to the simple shape of the BFD-curve (forcing function) and the constraints it imposes on the upper boundary conditions. Another likely contributing factor to (4) (as well as the other 3 issues) is the ash layer that formed during the fire. A month after the fire, the ash layer measured between 0.5 and 8 cm deep within the burn area and was about 2 cm deep over the area where the sensors were buried. Because the ash layer would have insulated the soil surface, it would have acted to slow the rate of cooling as the fire died out.

4.3 Soil Heat Flux

Comparisons between measured and modeled heat fluxes, Figure 7, are an independent check of the mathematical structure and tuning parameters of the surface forcing function, $Q_F(t)$. For this study $Q_F(t)$ was tuned primarily for soil temperatures and secondarily for soil heat flux. Figure 7 compares the observed heat fluxes (blue color-filled area and symbols) to the modeled heat fluxes (solid lines). The upper boundary of the (2 cm) blue color-filled region is the heat flux measured by the heat flux
465 plate without the Philip correction. The lower boundary of this region is the measured heat flux with the Philip correction, indicating that for this experiment the Philip correction reduced the amplitude of the uncorrected flux. The Philip correction is not shown for the two lower heat flux measurements (symbols) because it made virtually no change to the uncorrected fluxes. In general, the model does appear to capture many features of the observations. Of particular interest is that the amplitude of the modeled heat flux more closely agrees well with the Philip-corrected heat flux, providing confidence in both the model's
470 performance and the quality of the soil heat flux data. On the other hand, the modeled heat flux peaks several hours before the measured heat fluxes do. Without significantly increasing the complexity of the forcing function and the concomitant tuning effort, it is (at best) unlikely (if possible at all) to improve much on the model's ability to reproduce the observed temperature and heat flux data for this burn.

4.4 Soil Moisture

475 The modeled soil moisture is shown as a function of time in both Figures 8 and 9 for the same depths (and color-coding) as shown for temperature in Figure 6. Included on each figure is the soil moisture measured at 5 cm (red) and 15 cm (magenta)

depths; but Figure 8 includes the temperature-corrected calibration of the soil moisture probe, whereas Figure 9 does not. The red (5 cm) stars are interpolated values, which replace values that were flagged by the noise filter as questionable. Nonetheless, confidence in the fidelity of these interpolated values is high. But confidence in the magenta (15 cm) stars (also interpolated)

480   is less. Rather interestingly the modeled 5 cm soil moisture agrees better with temperature-corrected soil moisture, whereas at 15 cm the model resembles the uncorrected 15 cm soil moisture. Consequently, both figures are included here to show the importance of the temperature effects on the high-temperature TDR and to provide an estimate on the uncertainty inherent in these soil moisture measurements.

Figure 10 shows the observed (temperature-corrected) soil moisture versus the observed temperature along with the model's

485   solutions of θ vs T (or the model's $\theta - T$ trajectory). Here the model predicts that for depths less than 5 cm the soil moisture begins to evaporate (decrease) between 50 C and 90 C and that these initial evaporative temperatures increase deeper into the soil. Nonetheless, the model suggests that the soil does not dry out completely until temperatures have reached about 200 C. The observations at 5 cm show a similar pattern to the model, except these observations suggest that the initial evaporation stage proceeds more slowly and that overall evaporation occurs at a higher temperature. The same observation was made by

490   Massman (2012) and Massman (2015) regarding the laboratory data of Campbell et al. (1995). Several test simulations were performed to see if the model could be made to better emulate the observed $\theta - T$ trajectory, including: different formulations and parameter values for the hydraulic conductivity (K_R), different parameter values for the forcing function, $Q_F(t)$, and the simplified surface energy boundary condition, Equation (18), different WRCs, variations in the parameters of the source term, S_v, and removing the enhancement factor from the vapor diffusivity, D_{ve} and Equation (4). Only changes to S_v and D_{ve}

495   made any significant positive difference to the model's $\theta - T$ trajectory. Changes in either of these model factors can strongly influence the amount of vapor within the soil pores, in turn influencing the soil moisture dynamics. This should not be too surprising in the case of S_v, because S_v is formulated within the present model as a balance between the physical processes that govern evaporation and condensation to and from soil surfaces, and therefore influences the balance between soil moisture and soil vapor. In the case of reducing the enhancement factor (i.e., assigning it a value of 1), the resulting decrease in vapor

500   diffusivity causes the vapor within the soil pores to increases such that it feedbacks to soil moisture via the condensation term of S_v (proportional to ρ_v, Equation (9)), and again influencing the balance between θ and ρ_v. This exploration of the modeled and observed $\theta - T$ trajectory has yielded some insights into what maintains the long evaporative tail (where some soil moisture persists well past the boiling point of water), an issue that was less understood in Massman (2012) and Massman (2015).

Taken in total the model's simulation of soil moisture agrees with the observations fairly well. It is, of course, possible to

505   improve on the model's fidelity to the observations by adjusting the hydraulic function (K_R) or changing in the heating rates or duration and magnitude, $Q_F(t)$, and most importantly, by changing the values of the parameters of S_v and D_{ve} that influence soil vapor, ρ_v; but usually this comes at some expense to the model's fidelity to the measured soil temperatures. The same issue was noted in Massman (2012) and Massman (2015). Thus the present choice of model parameters is a compromise between two or three somewhat conflicting goals: fidelity to the soil's thermal response to heating by fire and the soil's moisture and

510   vapor response.

4.5 Dynamic Feedbacks

Fire changes soil and the more intense the fire and the greater amount of soil heating, the greater will be the changes in the soil. Examples of some of the changes that are relevant to the present study include (a) changes the soil bulk density (Butters , 2009; Kojima et al. , 2018), which will alter the WRC (figure 1) and hydraulic properties (Tian et al. , 2018), (b) changes to the thermal conductivity of the soil (Massman et al. , 2008; Kojima et al. , 2018) and the volumetric specific heat (Butters , 2009), (c) changes to the heat and vapor fluxes resulting from (a) and (b) (Kojima et al. , 2018), and (d) changes to the soil's specific surface area, A_{wa}, and particle surface potentials, which result when the fire induces water repellency in soils (Chen et al. , 2018). None of the physical/chemical processes causing these phenomena are included in any extant model of soil heating during fires. Part of the difficulty is that these are dynamic feedbacks occur during fires, consequently they influence soil heating and moisture transport in-situ during the fire. To give some idea of how these dynamic feedbacks may influence the soil heat and moisture transport, this section details the results of a model simulation based on observed or inferred changes to the bulk density and key thermophysical parameters.

The following model parameters were changed for this sensitivity analysis to feedbacks: soil bulk density increases from $1.30\,\mathrm{Mg\,m^{-3}}$ to $1.46\,\mathrm{Mg\,m^{-3}}$ (a 12% increase as per figure 1); the thermal conductivity of the mineral fraction, λ_{m0}, increases from $4.42\,\mathrm{Wm\,K^{-1}}$ to $8\,\mathrm{Wm\,K^{-1}}$, the de Vries shape factor, g_a, decreased from 0.123 to 0.06, the Campbell et al. (1994) parameter q_{w0} (which determines when water content starts to influence the soil's thermal conductivity) decreased from 0.03 to 0.02, the soil's volumetric specific heat increases by 10% (in accordance with the observations made by Butters (2009)), the overall soil thermal conductivity, λ_s, increases by 15%, and finally the source term coefficient, S_*, decreases from 0.1 to 0.08 (specifically chosen to be a 20% decrease). This increase in bulk density yields a concomitant decrease in soil porosity, η, which is simply carried over in a purely linear fashion to the WRC, the hydraulic function, and the source term, S_v. On its own this decrease in η yields an increase in S_v, so S_* is reduced to compensate for the decrease in A_{wa} suggested by Chen et al. (2018). It very natural to expect the soil's thermal conductivity to increase with the increase in bulk density, but the present model of thermal conductivity does not explicitly include any dependency on ρ_b. So λ_s is increased by 15% to accord with the increase predicted by the model developed by Johansen (1975). Changes to g_a and q_{w0} are intended to capture the observation (Massman et al. , 2008) that the fire decreased the sensitivity of the soil's thermal conductivity, λ_s, to soil moisture, (i.e., $\partial\lambda_s/\partial\theta$ decreased as a result of the fire) and increased λ_s when the soil is dry ($\theta < 0.08$). Decreasing g_a and q_{w0} was the best way to capture this pair of observations. In addition a decrease in g_a was also observed by Smits et al. (2016) for fire-affected soils. The conductivity of the mineral fraction, λ_m, was increased to capture the creation of thin, but highly conductive, coatings of mineral oxides (MnO_2 in particular) on the soil particle surfaces during the MEF experimental burn (Massman et al. , 2010b; Nobles et al. , 2010). Such thin coatings are synthetically created for routine application to nanotechnologies (e.g., O'Brian et al. , 2013).

The base case model simulation (Figs. 6, 7, 8, 9, 10) and the feedback simulation are compared in Figures 11, 12 and 13. The upper boundaries of the color-filled areas in Figures 11 (temperature) and 12 (heat flux) correspond to the feedback simulation. Whereas, the lower boundary in Figure 13 (soil volumetric moisture) is associated with the feedback simulation. These com-

545 parisons demonstrate that the feedbacks overwhelmingly act to increase the soil temperatures and heat fluxes throughout the soil and to significantly increase evaporation and evaporative losses of soil moisture (at least within the upper few centimeters of soil). However, the change in bulk density alone is responsible for about half of the differences shown in these figures. Overall though, these last three figures indicate that these dynamic feedbacks are potentially quite significant to the magnitude and depth of the soil heating. Or paraphrasing somewhat, during a fire soil temperatures are not a direct linear response to the

550 surface forcing function, rather at any given moment the soil heating feedbacks (non-linearly) upon itself creating conditions that allow the heat to penetrate more deeply into the soil and the soil temperatures to exceed what they would have been without the feedbacks.

5 Improving physical realism: Future observational and modeling studies

Although the HMV-model gives reasonably realistic simulations of soil temperatures and moisture during fires, there are several

555 enhancements that may further improve its performance and that should be useful to consider for future studies of the soil's response to heating during fires.

(a) Dynamic Feedbacks and Soil Thermal Conductivity. A better physical understanding of the dynamical processes that govern how extreme heating during fires changes ρ_b and the development of a model of λ_s that captures this dynamic. Also a better formulation of how soil structure influences g_a and λ_s and how soil structure changes during a fire. This issue of

560 improving model parameterizations of λ_s is more complex that just including ρ_b because the observed increase in λ_s for a dry soil was 200-300% (Massman et al. , 2008), which far exceeds the 15-17% predicted by the model of Johansen (1975).

(b) Mass Transport. The present version of the HMV-model assumes an advective transport of water vapor induced by the rapid volitalization of the soil moisture, u_{vl} and Equation (5). But most formulations of advective transport in soils are based on Darcy's law. For application to fire u_{vl} from Darcy's law would result from the rapidly evolving vapor pressure and

565 temperature gradients. Additionally it would be worthwhile to include the dry air density, ρ_d, as a separate model variable. Certainly in any real fire the temperature and pressure of the dry air within the soil pore spaces would respond dynamically to heating. But including ρ_d as a dynamic variable should yield a more physically realistic simulation of the diffusional and advective transport of water vapor during the fire. Finally, given the potential for extreme gradients in soil water potential and temperature during fires, it may also be worthwhile to include the heat transported by the movement of water (e.g., Stallman ,

570 1965; Pasquale et al. , 2014) in Equation (1). This energy transport term has often been included when modeling the daily cycle of energy flow through soils. Because some fires, especially slash pile burns, can continue a week or more, it seems appropriate to investigate the influence this type of energy transport could have on model solutions.

(c) 2- and 3-Dimensional Effects. There are (at least) two physical processes that cannot be fully represented in a 1-d model: (*i*) horizontal heat flux (G_{hor}) and (*ii*) possible advective currents (here characterized by an advective velocity u_{adv}) induced in

575 the soil shortly after the pile is ignited ((Massman et al. , 2010a; Nobles et al. , 2010; Massman et al. , 2010b)). (*i*) In an earlier section mention was made of the second installation of soil sensors at the edge of the pile. These data used in conjunction with the soil temperature data at the center of the pile it is possible to obtain a crude estimate of the horizontal temperature gradient.

Then assuming that horizontal and vertical thermal conductivities (at the same depth) are about the same in magnitude, it is possible to show that G_{hor} during the fire is approximately 10% of the vertical soil heat flux. This estimate of G_{hor} was

580 confirmed with data taken during another experimental burn performed in the fall of 2004, in which the 20 or so temperature sensors were placed in a horizontal array that allowed about 20 different horizontal gradients to be compared with about the same number of vertical gradients. This is relevant to the present study because it may help explain some of the divergence between modeled and observed soil temperatures and (vertical) heat fluxes and further underscores the nature of the challenges and empiricism inherent in modeling of soil heating during fires. (*ii*) Far more important for any further studies is the possibility

585 of a fire-induced u_{adv} because it appears to be inherently 2- or 3-dimensional in nature and to carry combustion products into the soil (Massman et al. , 2010b, figure 4). Such an advective current is hypothesized to have caused the extremely rapid 20-fold increase in soil CO_2 observed to have occurred within the first 30 minutes of the Manitou burn being modeled here (Massman et al. , 2010a). Consequently, any combustion-produced water vapor will also be transported. If this is the case it would likely overwhelms u_{vl} and contradict assumptions made about evaporation at the soil surface and the transport of soil water vapor

590 during (at least) some portion of the burn. It may be possible to just impose u_{adv} in a 1-d model like the HMV-model, but such an adjustment should probably be guided by observational studies and experiments designed to establish the existence, nature and dynamics of u_{adv}.

6 Concluding Summary

This study describes the continuing development, improvement, and validation of the HMV-model, a non-equilibrium model

595 of the coupled transport of heat, moisture, and water vapor in soils during surface fires. The purpose of the research supporting this study is to provide a tool to aid in the management (and reduction, if possible) of the physical and ecological affects of fire on soils. Key improvements to the model, which noticeably improved its stability and performance, include more physically realistic parameterizations of the non-equilibrium vapor source term, S_v, and soil thermal conductivity, λ_s. Integral to the validation of this model are the development of a general surface heating (forcing) function and the discussions of the

600 complexities and difficulties regarding formulating the surface (or upper) boundary condition. The model is validated using in-situ measurements of soil temperatures, heat flux, and soil moisture obtained during a 2004 experimental burn carried out at Manitou Experimental Forest (in the central Rocky Mountains of Colorado). Despite any possible ambiguities in the calibration of the soil moisture and heat flux sensors and given the simplicity of the modeled forcing function and the complexities of the true forcing that can be inferred from the dynamics of the soil data, the model's ability to reproduce the observations is at

605 least reasonable, and maybe even surprisingly good. But as with Massman (2012) and Massman (2015), tuning the model parameters requires navigating the somewhat divergent goals of achieving a "best" fit to either the soil temperature observations or soil moisture observations. Absent to the model are important fire-induced feedbacks, in particular in-situ changes to the soil's thermal and hydraulic properties that are inevitable when the fire (as is often observed) causes the soil's bulk density to increase. This important dynamic was investigated with a model sensitivity analysis by making logical and credible changes in

610 the (appropriate) model parameters. The net affect of this feedback is that the heat pulse will propagate much deeper into the

soil than it would have otherwise, pointing to the need for further observational and modeling studies of this phenomenon. This study closes by highlighting other areas of research needed to improve our understanding of and ability to model the physical processes that occur in soils during fires, including issues involving the transport of both soil moisture and soil vapor during fires, the potentially very significant 2- or 3-dimensional advective flows in soils induced by fires, and the possibility of 2- or

615 3-dimensional heat flow.

Code and data availability. The computer code used in this study was developed using MatLab version 2017b and is publicly available along with any output data at the Forest Service Research Data Archive https://doi.org/10.2737/RDS-2020-YYYY. Prior to its availability online the code and any output is freely available from the author.

Appendix A: Soil Apparent Thermal Conductivity

620 **A1   Mass Gradient Diffusional Flux: $-D_{ve}\partial\rho_v/\partial z$**

de Vries (1958) defines the soil's apparent thermal conductivity, $\lambda_{s,app}$, as the medium's thermal conductivity "including the effect of the vapor distillation due to temperature gradients". But in a modeling context, the use of $\lambda_{s,app}$ has to be treated with some care because it is inappropriate to externally introduce $\lambda_{s,app}$ into the equation for conservation of energy (employed universally as part of any model of heat and moisture flow in soils). This appendix develops both an equilibrium and a non-

625 equilibrium model for $\lambda_{s,app}$ to illuminate its thermodynamic origins and to clarify its proper role in modeling of soil heat and moisture flow in soils. Before proceeding, note that all terms relating to advective vapor flow (i.e., u_{vl}) and liquid water flow (i.e., K_n, K_H and $V_{\theta,surf}$) can be ignored because they are superfluous for purposes of this appendix.

The basic conservation equations employed in this study are Equations (6), (7) and (4). But there is a valid alternative expression for Equation (6), which results by combining the conservation of enthalpy, Equation (1), with the conservation of

630 water vapor, Equation (4), and the equilibrium assumption ($\rho_v = \rho_{v,eq} = a_w\rho_{v,sat}$), and is expressed as

$$C_s\frac{\partial T}{\partial t} - \frac{\partial}{\partial z}\left[\lambda_s\frac{\partial T}{\partial z}\right] + L_v^*\frac{\partial(\eta-\theta)\rho_{v,eq}}{\partial t} - L_v^*\frac{\partial}{\partial z}\left[D_{ve}\frac{\partial\rho_{v,eq}}{\partial z}\right] = 0 \tag{A1}$$

which after some simple mathematical manipulation can also be written as

$$C_s\frac{\partial T}{\partial t} - L_v^*\rho_{v,eq}\frac{\partial\theta}{\partial t} + L_v^*(\eta-\theta)\frac{\partial\rho_{v,eq}}{\partial t} - \frac{\partial}{\partial z}\left[\lambda_s\frac{\partial T}{\partial z} + L_v^*D_{ve}\frac{\partial\rho_{v,eq}}{\partial z}\right] + D_{ve}\frac{\partial\rho_{v,eq}}{\partial z}\frac{\partial L_v^*}{\partial z} = 0 \tag{A2}$$

where the last term on the right hand side of this equation accounts for moving L_v^* inside the gradient operator $\partial/\partial z$. As

635 discussed in the main text $a_w = a_w(T_K,\psi)$ is modeled by the Kelvin Equation, $a_w = e^{\frac{M_w\psi_*}{RT_K}}\psi_n$, and $\rho_{v,sat} = \rho_{v,sat}(T_K)$, so

that $\partial\rho_{v,eq}/\partial t$ can be expanded in terms of $\partial T/\partial t$ and $\partial\psi_n/\partial t$ and $\partial\rho_{v,eq}/\partial z$ in terms of $\partial T/\partial z$ and $\partial\psi_n/\partial z$. The following shows $\partial\rho_{v,eq}/\partial z$. (Note $\partial\rho_{v,eq}/\partial t$ can be found by substituting t for z).

$$\frac{\partial\rho_{v,eq}}{\partial z} = \left[a_w\Delta_{sat} - a_w\left(\frac{M_w\psi_*\psi_n}{RT_K}\right)\frac{\rho_{v,sat}}{T_K}\right]\frac{\partial T}{\partial z} + \left[a_w\left(\frac{M_w\psi_*}{RT_K}\right)\rho_{v,sat}\right]\frac{\partial\psi_n}{\partial z} \tag{A3}$$

where Δ_{sat} (kgm^{-3}K^{-1}) is the slope of the saturation vapor curve, $d\rho_{v,sat}/dT$, and $7\times10^{-4} < \Delta_{sat} < 70\times10^{-4}$ for temper-
640 atures between about 5 and 60C. Furthermore, unless the soil is extremely dry $(\psi_n\approx 1)$ $-[(M_w\psi_*\psi_n)/(RT_K)][\rho_{v,sat}/T_K] \ll \Delta_{sat}$; implying that the second term multiplying the temperature gradient of Equation (A3) can be ignored relative to the first term for most applications. Otherwise for an extremely dry soil $-[(M_w\psi_*\psi_n)/(RT_K)][\rho_{v,sat}/T_K] \approx 0.5\Delta_{sat}$. Henceforth $\Delta_{sat}^* \equiv \Delta_{sat} - [(M_w\psi_*\psi_n)/(RT_K)][\rho_{v,sat}/T_K]$. In addition, it is always true that $(\psi_n/T_K)\partial T/\partial z \gg \partial\psi_n/\partial z$, which means that the rightmost term in Equation (A3) can also be ignored. Therefore, Equation (A3) is now

645 $$\frac{\partial\rho_{v,eq}}{\partial z} = a_w\Delta_{sat}^*\frac{\partial T}{\partial z} \tag{A4}$$

Substituting Equation (A4) into Equation (A2) yields

$$C_s\frac{\partial T}{\partial t} - L_v^*\rho_{v,eq}\frac{\partial\theta}{\partial t} - \frac{\partial}{\partial z}\left[(\lambda_s + a_wL_v^*D_{ve}\Delta_{sat}^*)\frac{\partial T}{\partial z}\right] + D_{ve}\frac{\partial\rho_{v,eq}}{\partial z}\frac{\partial L_v^*}{\partial z} = 0 \tag{A5}$$

where the term $L_v^*(\eta-\theta)\partial\rho_{v,eq}/\partial t$ has been dropped from Equation (A2) because $|L_v^*(\eta-\theta)\partial\rho_{v,eq}/\partial t| \ll |C_s\partial T/\partial t|$ (although it is a bit tedious to show). Equation (A5) yields the following identification for $\lambda_{s,app}$:

650 $$\lambda_{s,app} = \lambda_s + a_wL_v^*D_{ve}\Delta_{sat}^* = \lambda_s + \lambda_{s,dis} \tag{A6}$$

where the term describing "the effect of the vapor distillation due to temperature gradients" on the soil's thermal conductivity is $a_wL_v^*D_{ve}\Delta_{sat}^*$ (identified in Equation (A6) as $\lambda_{s,dis}$). This expression for $\lambda_{s,app}$ is often used as the justification for including the effects of vapor transfer on λ_s, i.e., the substitution of $\lambda_{s,app}$ for λ_s in the equation of conservation of enthalpy in soils ((e.g., Hillel , 2004, Equation (12.24), p. 226) and (Campbell et al. , 1995; Smits et al. , 2011; Massman , 2015)). But as
655 this appendix shows, in a modeling context, this substitution is usually unnecessary (and inappropriate) because these vapor transfer effects are already either directly or indirectly embedded in the equation for conservation of enthalpy.

Next is the introduction of the equilibrium assumption, Equation (A4), into Equation (7). This yields

$$(\rho_w - \rho_{v,eq})\frac{\partial\theta}{\partial t} + (\eta-\theta)\frac{\partial\rho_{v,eq}}{\partial t} + \frac{\partial}{\partial z}\left[a_wD_{ve}\Delta_{sat}^*\frac{\partial T}{\partial z}\right] = 0 \tag{A7}$$

or to a very good approximation (which follows from Equation (A7) because $\rho_w \gg \rho_{v,eq}$)

660 $$\rho_w\frac{\partial\theta}{\partial t} + (\eta-\theta)\frac{\partial\rho_{v,eq}}{\partial t} + \frac{\partial}{\partial z}\left[a_wD_{ve}\Delta_{sat}^*\frac{\partial T}{\partial z}\right] = 0 \tag{A8}$$

Equations (A5) and (A8) now form an equilibrium model with two independent predictive variables (T and θ or ψ) that describes the coupled heat and moisture flow in soils. This particular model clearly results in and is completely consistent with the soil's apparent thermal conductivity, $\lambda_{s,app}$. On the other hand, there is an equally valid model of this coupled dual-variable model for which $\lambda_{s,app}$ is not only unnecessary, but it would, in fact, an error to invoke its use with the model.

665 This other coupled heat and moisture flow model combines the conservation of mass for water (liquid + vapor), Equation (A8) above, with the simplified version of the conservation of energy equation, Equation (6), discussed in the development of the non-equilibrium model. This simplified equation is

$$C_s\frac{\partial T}{\partial t} - \frac{\partial}{\partial z}\left[\lambda_s\frac{\partial T}{\partial z}\right] - L_v^*\rho_w\frac{\partial \theta}{\partial t} = 0 \qquad (A9)$$

It is important to reiterate that the paired Equations (A8) and (A5) are as valid a basis for describing coupled heat and
670 moisture flow in soils as are the paired Equations (A8) and (A9); although Equations (A8) and (A9) are much more extensively used. But the conservation of energy equation as expressed with Equation (A9) does not explicitly include "the effect of the vapor distillation due to temperature gradients" ($\lambda_{s,dis}$), whereas Equation (A5) does. Rather the effects of distillation of water vapor are implicit in Equation (A9) because they are included in $\partial\theta/\partial t$ (via Equation (A8)). Therefore, to substitute $\lambda_{s,app}$ for λ_s in Equation (A9) or any θ-based variant of Equation (A9) (as opposed to a ρ_v-based variant like Equation (A5)) on the
675 assumption that λ_s should explicitly include the effects of water distillation, is incorrect because to do so is to double count the effects of $\lambda_{s,dis}$ on soil thermal energy transport. This double counting is even more obvious (using the same argument that λ_s should include the $\lambda_{s,dis}$ term) when $\lambda_{s,app}$ is substituted for λ_s in Equation (A5), which already explicitly includes $\lambda_{s,dis}$.

The non-equilibrium form of $\lambda_{s,app}$ follows from the same general methodology as the equilibrium form does from Equation (A5). First, combining Equations (1) and (4) and then simplifying yields

$$680 \quad C_s\frac{\partial T}{\partial t} - L_v^*\rho_v\frac{\partial \theta}{\partial t} - \frac{\partial}{\partial z}\left[\lambda_s\frac{\partial T}{\partial z} - L_v^*D_{ve}\frac{\partial \rho_v}{\partial z}\right] + D_{ve}\frac{\partial \rho_v}{\partial z}\frac{\partial L_v^*}{\partial z} = 0 \qquad (A10)$$

Next employing the ideal gas law for ρ_v, i.e., $e_v = \rho_v RT_K/M_w$ yields

$$\frac{\partial \rho_v}{\partial z} = -\frac{\rho_v}{T_K}\frac{\partial T}{\partial z} + \frac{M_w}{RT_K}\frac{\partial e_v}{\partial z} \qquad (A11)$$

Finally introducing Equation (A11) into Equation (A10) yields

$$C_s\frac{\partial T}{\partial t} - L_v^*\rho_v\frac{\partial \theta}{\partial t} - \frac{\partial}{\partial z}\left[\left(\lambda_s + L_v^*D_{ve}\frac{\rho_v}{T_K}\right)\frac{\partial T}{\partial z}\right] + \frac{\partial}{\partial z}\left[\left(\frac{L_v^*D_{ve}M_w}{RT_K}\right)\frac{\partial e_v}{\partial z}\right] + D_{ve}\frac{\partial \rho_v}{\partial z}\frac{\partial L_v^*}{\partial z} = 0 \qquad (A12)$$

685 where now the non-equilibrium form of $\lambda_{s,dis}$ is $L_v^*D_{ve}\rho_v/T_K$. For practical applications this is obviously not as convenient or as useful as the equilibrium form because $\lambda_{s,dis}$ is now a function of ρ_v, which for most experimental settings in soils is difficult (if not impossible) to measure directly. Nonetheless, for the purposes of this appendix, it suffices to show that a

non-equilibrium model of $\lambda_{s,dis}$ can be defined and that in a modeling context it is just as unnecessary and inappropriate to use as is the better known equilibrium version of $\lambda_{s,dis}$.

690   Summarizing and concluding: The conservation of enthalpy (Equation (1), or one of its many derivatives, e.g., Equations (6), (A5), (A9)), is fundamental to all models of heat and moisture flow in soils. All forms of this conservation law also explicitly include the effects of the phase change of water through the vapor source term, $L_v^* S_v$. Therefore, all effects associated with the distillation of water are a result of S_v. This is true whether discussing an equilibrium or non-equilibrium model. Imposing or assuming liquid/vapor equilibrium or non-equilibrium has mathematical consequences to how ρ_v and S_v are parameterized and

695 can also have indirect influence on the soil's intrinsic thermal conductivity (λ_s), because λ_s is a function of several variables, among which are soil volumetric water content and soil vapor density, i.e., $\lambda_s = \lambda_s(\theta, \rho_v, \cdots)$ (de Vries (1963); Campbell et al. (1994); Tian et al. (2016)). But within a modeling context there is no justification for substituting the apparent thermal conductivity, $\lambda_{s,app}$, for the soil's intrinsic thermal conductivity, λ_s, in the equation of conservation of enthalpy, Equation (1). To do so violates the conservation of enthalpy by effectively double counting $\lambda_{s,dis}$.

700 **A2   Mass Mixing Ratio Diffusional Flux: $-\rho_a D_{ve} \partial \chi_v / \partial z$**

The discussion in this section of the appendix complements the discussion of λ_{app} and $\lambda_{s,dis}$ in A1 above. It does not change the final outcome or conclusions reached in A1. A2 is included here only to further refine $\lambda_{s,dis}$. Furthermore, results of this section are limited to relatively moist soils, for which $\lambda_{s,dis}$ is of greatest interest and significance.

    The discussion in A1 above develops $\lambda_{s,app}$ more-or-less along the traditional lines, using the mass gradient form of the

705 diffusional flux, $-D_{ve}\partial\rho_v/\partial z$. But the diffusional flux is also represented (and sometimes more appropriately represented) in terms of the gradient of the mass mixing ratio, i.e., $-\rho_a D_{ve}\partial\chi_v/\partial z$; where ρ_a (kgm^{-3}) is the total (dry air + vapor) soil gas density and χ_v (kgkg^{-1}) $= \rho_v/\rho_a$. This section of the appendix shows that for a relatively moist soil (i.e., $a_w \approx 1$ and $\chi_{v,eq} \approx \chi_{v,sat}$) $\lambda_{s,dis}$ developed in A1 above differs between +2.5% (for $T \approx 5$ C) and -4.5% (for temperatures $T \approx 60$ C) from that given in Equation (A6). All that this requires is to show how $\rho_a \partial \chi_{v,eq}/\partial z$ generalizes Equation (A4).

710   From the identity $\rho_a = \rho_d + \rho_{v,eq}$, where ρ_d (kgm^{-3}) is the soil dry air density, it follows that

$$\rho_a \frac{\partial \chi_{v,eq}}{\partial z} = (\rho_d + \rho_{v,eq}) \frac{\partial}{\partial z}\left(\frac{\rho_{v,eq}}{\rho_d + \rho_{v,eq}}\right) = \frac{\partial \rho_{v,eq}}{\partial z} - \chi_{v,eq}\frac{\partial(\rho_d + \rho_{v,eq})}{\partial z} \qquad (A13)$$

Next, assuming that ρ_d is an ideal gas it follows that

$$\frac{\partial \rho_d}{\partial z} = \frac{\rho_d}{p_d}\frac{\partial p_d}{\partial z} - \frac{\rho_d}{T_K}\frac{\partial T}{\partial z} \qquad (A14)$$

Because the pressure gradient term, $(\rho_d/p_d)\partial p_d/\partial z$, is not relevant for the present purposes (and it is unlikely to contribute

715 much to $\partial\rho_d/\partial z$ anyway) it can be dropped from Equation (A14). This yields

$$\rho_a \frac{\partial \chi_{v,eq}}{\partial z} = (1 - \chi_{v,eq})\frac{\partial \rho_{v,eq}}{\partial z} + \chi_{v,eq}\frac{(\rho_a - \rho_{v,eq})}{T_K}\frac{\partial T}{\partial z} \qquad (A15)$$

which after combining with Equation (A4) and some further simplification yields

$$\rho_a \frac{\partial \chi_{v,eq}}{\partial z} = (1 - \chi_{v,eq}) a_w \left(\Delta^*_{sat} + \frac{\rho_{v,sat}}{T_K} \right) \frac{\partial T}{\partial z} \tag{A16}$$

from which it follows that

720
$$\lambda_{s,dis} = L^*_v D_{ve} a_w (1 - \chi_{v,eq}) \left(\Delta^*_{sat} + \frac{\rho_{v,sat}}{T_K} \right) \tag{A17}$$

This last expression indicates that there are two (moderately) compensating terms to $\lambda_{s,dis}$ that do not occur in the diffusional mass flux form for the apparent thermal conductivity. These are $(1 - \chi_{v,eq})$ instead of 1 and $\Delta^*_{sat} + \rho_{v,sat}/T_K$ instead of Δ^*_{sat}. At about 5 C $\chi_v \approx 0.005$ and $\rho_{v,sat}/T_K \approx 0.03\Delta^*_{sat}$. Whereas at 60 C $\chi_v \approx 0.10$ and $\rho_{v,sat}/T_K \approx 0.06\Delta^*_{sat}$. These results imply that at 5 C Equation (A17) will yield a value for $\lambda_{s,dis}$ that is about 2.5% higher than $\lambda_{s,dis} = L^*_v D_{ve} a_w \Delta^*_{sat}$ and that

725 near 60 C Equation (A17) yields a value for $\lambda_{s,dis}$ that is about 4.5% lower. Unless a correction between +2% and -4.5% is important for estimating $\lambda_{s,dis}$, then it seems that the mass mixing ratio formulation for the diffusional mass flux, Equation (A17), adds very little value to the original formulation, Equation (A6).

Author contributions. W. J. Massman is the sole author of this paper.

Competing interests. The author declares no competing interests.

730 *Acknowledgements.* The author would like to thank Dr M. Novak for his continued interest in this research and for many discussions on various aspects of this work. I would also like to thank Dr G. Kuitenberg for sharing his time for discussions on all aspects of soil physics relevant to the research discussed in this manuscript.

References

Abatzogloua, J. T., and Williams, A. P.: Impact of anthropogenic climate change on wildfire across western US forests, Proc. Natl. Acad. Sci. USA, 113(42), 11770–11775, doi:10.1073/pnas.1607171113, 2016.

Arya, L. M., Leij, F. J., van Genuchten, M. Th., and Shouse, P. J.: Scaling parameter to predict the soil water characteristic from particle-size distribution data, Soil Sci. Soc. Am. J., 63, 510–519, doi:10.2136/sssaj1999.03615995006300030013x, 1999.

Assouline, S.: A model for the relative hydraulic conductivity based on the water retention curve, Water Resour. Res, 37, 265–271, doi:10.1029/2000WR900254, 2001.

Barnett, C. R.: BFD curve: A new empirical model for fire compartment temperatures, Fire Safety Journal, 37, 437–463, doi:10.1016/S0379-7112(02)00006-1, 2002.

Bauer, T. H.: A general analytical approach toward the thermal conductivity of porous media, Int. J. Heat Mass Tran., 36, 4181–4191, doi:10.1016/0017-9310(93)90080-P, 1993.

Bear, J.: Dynamics of Fluids in Porous Media, American Elsevier Pub. Co, New York, NY, USA, ISBN-13 978-0-486-65675-5, ISBN-10 0-486-65675-6, 1972.

Blagojevič, M. D. and Pešič, D. J.: A new curve for temperature-time relationship in compartment fire, Thermal Science, 5(2), 339–352, doi:10.2298/tsci100927021B, 2011.

Borujerdi, P. R., Shotorban, B., Mahalingam, S., and Weise, D. R.: Modeling of water evaporation from a shrinking moist biomass slab subject to heating: Arrhenius approach versus equilibrium approach, Int. J. Heat Mass Tran., 145, 118672, doi:10.1016/j.ijheatmasstransfer.2019.118672, 2019.

Brutsaert, W.: Evaporation into the atmosphere: Theory, history and applications, D.Reidel Publishing Co., Dordrecht, The Netherlands, doi:10.1007/978-94-017-1497-6, 1984.

Brusseau, M. L., Peng, S., Schnaar, G., and Costanza-Robinson., M. S.: Relationships among air-water interfacial area, capillary pressure, and water saturation for a sandy porous medium. Water Resources Research, 42, W03501. doi:10.1029/2005WR004058, 2006.

Butters, G.: Personal Communication, 2009.

Campbell, G. S., and Shiozawa, S.: Prediction of hydraulic properties of soils using particle-size distribution and bulk density data, in Indirect methods for estimating the hydraulic properties of unsaturated soils, edited by M. Th. van Genuchten, University of California, Riverside, CA, 317–328, 1992.

Campbell, G. S., Jungbauer Jr., J. D., Bidlake, W. R., and Hungerford, R. D.: Predicting the effect of temperature on soil thermal conductivity, Soil Science, 158, 307–313, doi:10.1097/00010694-199411000-00001, 1994.

Campbell, G. S., Jungbauer Jr., J. D., Bristow, K. L., and Hungerford, R. D.: Soil temperature and water content beneath a surface fire, Soil Science, 159(6), 363–374, doi:10.1097/00010694-199506000-00001, 1995.

Chen, J., Shang, C., Eick, M. J., and Stewart, R. D.: Water repellency decreases vapor sorption of clay minerals, Water Resour. Res., 55, 6114–6125, doi:10.1029/2018WR023352, 2018.

de Vries, D. A.: Thermal properties in soils, in: Physics of Plant Environment, edited by: van Wijk, W. R., North Holland Publishing Co., Amsterdam, The Netherlands, 201–255, 1963.

de Vries, D. A.: Simultaneous heat and moisture transfer in porous media, EOS Trans. AGU, 39, 909–916, doi:10.1029/TR039i005p00909, 1958.

Dey, D. C., and Schweitzer, C. J.: A Review on the dynamics of prescribed fire, tree mortality, and injury in managing oak natural communities to minimize economic loss in North America, Forests, 9, 461, doi:10.3390/f9080461, 2018.

Finney, M. A., Cohen, J. D., Forthofer, J. M., McAllister, S. S., Gollner, M. J., Gorham, D. J., Saito, K., Akafuah, N. K., Adam, B. A., and English, D. D.: Role of buoyant flame dynamics in wildfire spread, Proc. Natl. Acad. Sci. USA, 112(32), 9833–9838, doi:10.1073/pnas.1504498112, 2015.

Fredlund, D. G., and Xing, A.: Equations for the soil-water characteristic curve, Can. Geotech. J., 31, 521–532, doi:10.1139/t94-061, 1994.

Grant, S. A.: Extension of a temperature effects model for capillary pressure saturation relations, Water Resour. Res., 39(1), 1003, doi:10.1029/2000WR000193, 2003.

Groenevelt, P. H. and Grant, C. D.: A new model for the soil-water retention curve that solves the problem of residual water contents, European J. Soil Sci., 55, doi:10.1111/j.1365-2389.2004.00617.x, 79–485, 2004.

Harrison, S. P., Marlon, J. R., and Bartlein, P. J.: Fire in the earth system, in: Changing Climates, Earth Systems and Society, International Year of Planet Earth, edited by: J. Dodson, Springer-Verlag, Berlin, Germany, 21–48, doi:10.1007/978-90-481-8716-4_3, 2010.

Hillel, D.: Introduction to environmental soil physics, Elsevier Academic Press, Amsterdam, The Netherlands, 2004.

Kanamori, H., Fujii, N., and Mizutani, H.: Thermal diffusivity measurement of rock-forming minerals from $300°$ to $1100°$ K, J. Geophys. Res., 73, 595–605, doi:10.1029/JB073i002p00595, 1968.

Kasischke, E. S., and Turetsky, M. R.: Recent changes in the fire regime across the North American boreal region–Spatial and temporal patterns of burning across Canada and Alaska, Geophys. Res. Lett., 33, L09703, doi:10.1029/2006GL025677, 2006.

Johansen, O.: Thermal conductivity of soils, PhD thesis, Institutt for kjoleteknikk, Trondheim, Norway, 291 pp., 1975. (Available as US-ACRREL Draft Translation 637, 1977.)

Kojima, Y., Heitman, J. L., Sakai, M., Kato, C., and Horton, R.: Bulk density effects on soil hydrologic and thermal characteristics: A numerical investigation, Hydrological Processes, 32, 2203–2216, doi:10.1002/hyp.13152, 2018.

Linn, R.: Fluid dynamics of wildfires, Physics Today, 72(11), 70–71, doi:10.1063/PT.3.4350, 2019.

Lutz, J. F., and Kemper, W. D.: Intrinsic permeability of clay as affected by clay-water interaction, Soil Science, 88(2), 83–90, doi:10.1097/00010694-195988020-00005, 1959.

Massman, W. J.: Modeling soil heating and moisture transport under extreme conditions: Forest fires and slash pile burns, Water Resour. Res., 48, W10548, doi:10.1029/2011WR011710, 2012.

Massman, W. J.: A non-equilibrium model for soil heating and moisture transport during extreme surface heating: the soil (heat-moisture-vapor) HMV-Model Version 1, Geosci. Model Dev., 8, 3659–3680, doi:10.5194/gmd-8-3659-2015, 2015.

Massman, W. J., and Frank, J. M.: Effect of a controlled burn on the thermophysical properties of a dry soil using a new model of soil heat flow and a new high temperature heat flux plate, Int. J. Wildland Fire, 13, 427–442, doi:10.1071/WF04018, 2004.

Massman, W. J., Frank, J. M., Jiménez Esquilin, A. E., Stromberger, M. E., and Shepperd, W. D.: Long term consequences of a controlled slash burn and slash mastication to soil moisture and CO_2 at a southern Colorado site, in: 27th Conference on Agricultural and Forest Meteorology, 22-25 May 2006, San Diego, CA, paper 2.2 (available on CD from the AMS and at http://ams.confex.com/ams/BLTAgFBioA/techprogram/programexpanded_352.htm), 2006.

Massman, W. J., Frank, J. M., and Mooney, S. J.: Advancing investigation and modeling of first-order fire effects on soils, Fire Ecology, 6, 36–54, doi:10.4996fireecology0601036, 2010

Massman, W. J., Frank, J. M., and Reisch, N. B.: Long term impacts of prescribed burns on soil thermal conductivity and soil heating at a Colorado Rocky Mountain site: a data/model fusion study, Int. J. Wildland Fire, 17, 131–146, doi:10.1071/WF06118, 2008.

Massman W. J., Nobles, M. M., Butters, G., and Mooney, S.: Transport of CO_2 and other combustion products in soils during slash-pile burns, in: VI International Conference on Forest Fire Research 2010 November 15-18 (Abstracts Volume and accompanying CD; ISBN 978-989-20-2157-7), edited by: Viegas, D. X., ADAI/CEIF, Coimbra, Portugal, Submission 086, 2010.

810 McCaffrey, S., Toman, E., Stidham, M., and Shindler, B.: Social Science Findings in the United States, in: Wildfire Hazards, Risks, and Disasters, edited by: Paton, D., Buergelt, P. T., McCaffrey, S., Tedim, F., and Shroder J. F., Elsevier, Amsterdam, Netherlands, 15–34, doi:10.1016/B978-0-12-410434-1.00002-6, 2015.

Millar, C. I., Stephenson, N. L., and Stephens, S. L.: Climate change and forests of the future: Managing in the face of uncertainty, Ecol. Appl., 17, 2145–2151, https://doi.org/10.1890/06-1715.1, 2007.

815 Moritz, M. A., Parisien, M.-A., Batllori, E., Krawchuk, M. A., Van Dorn, J., Ganz, D. J., and Hayhoe, K.: Climate change and disruptions to global fire activity, Ecosphere 3(6), 49, http://dx.doi.org/10.1890/ES11-00345.1, 2012.

Nobles, M. M., Massman W. J., Mbila, M., and Butters, G.: Mineralogical and micromorphological modifications in soil affected by slash pile burn, in: VI International Conference on Forest Fire Research 2010 November 15-18 (Abstracts Volume and accompanying CD; ISBN 978-989-20-2157-7), edited by: Viegas, D. X., ADAI/CEIF, Coimbra, Portugal, Submission 288, 2010.

820 Novak, M. D.: Comment on "Evaporation from soils under thermal boundary conditions: Experimental and modeling investigation to compare equilibrium- and nonequilibrium-based approaches" by Kathleen M. Smits, Abdullah Cihan, Toshihiro Sakaki, and Tissa H. Illangasekare, Water Resour. Res., 48, W05549, doi:10.1029/2011WR011393, 2012.

Novak, M. D.: Validity of assuming equilibrium between liquid water and vapor for simulating evaporation, Water Resour. Res., 55, doi:10.1029/2019WR025113, 2019.

825 O'Brian, P. J., Shenogin, S., Liu, J., Chow, P. K., Laurencin, D., Mutin, P. H., Yamaguchi, M., Keblinski, P., and Ramanath, G.: Bonding-induced thermal conductance enhancement at inorganic heterointerfaces using nanomolecular monolayers, Nature Materials, 12, 118–122, doi:10.1038/nmat3465, 2013.

Ouedraogo, F., Cherblanc, F., Naon, B., and Bénet, J.-C.: Water transfer in soil at low water content. Is the local equilibrium assumption still appropriate?, J. Hydrology, 492, 117–127, doi:10.1016/j.jhydrol.2013.04.004, 2013.

830 Pasquale, V., Verdoya, M., and Chiozzi, P.: Heat in the Groundwater Flow, in: Geothermics (Heat flow in the lithosphere), Springer, Dordrecht, The Netherlands, 101–116, doi:10.1007/978-3-319-02511-7_5, 2014.

Pearce, H. G., Finney, M., Strand, T., Katurji, M., and Clements, C.: New Zealand field-scale fire experiments to test convective heat transfer in wildland fires, Proceedings for the 6th International Fire Behavior and Fuels Conference April 29 - May 3, 2019, Sydney, Australia, International Association of Wildland Fire, Missoula, Montana, USA, 2019.

835 Philip, J. R.: The theory of heat flux meters, J. Geophys. Res., 66, 571–579, doi:10.1029/JZ066i002p00571, 1961.

Philip, J. R., and de Vries, D. A.: Moisture movement in porous materials under temperature gradients, EOS Trans. AGU, 38, 222–232, doi:10.1029/TR038i002p00222, 1957.

Prunty, L., and Bell, J.: Soil temperature change over time during infiltration, Soil Sci. Soc. Am. J., 69, 766–775, doi:10.2136/sssaj2004.0219, 2005.

840 San-Miguel-Ayanz, J., Durrant, T., Boca, R., Libertà, G., Branco, A., de Rigo, D., Ferrari, D., Maianti, P., Vivancos, T. A., Oom, D., Pfeiffer, H., Nuijten, D., and Leray, T.: Forest Fires in Europe, Middle East and North Africa 2018, EUR 29856 EN, ISBN 978-92-76-11234-1, doi:10.2760/1128, 2019.

Sauer, T. J., Meek, D. W., Ochsner, T. E., Harris, A. R., and Horton, R.: Errors in heat flux measurments in flux plates of contrasting design and thermal conductivity, Vadose Zone J., 2, 580–588, doi:10.2113/2.4.580, 2003.

845   Schoennagel, T., Balch, J. K., Brenkert-Smith, H., Dennison, P. E., Harvey, B. J., Krawchuk, M. A., Mietkiewicz, N., Morgan, P., Moritz, M. A., Rasker, R., Turner, M. G., and Whitlock, C.: Adapt to more wildfire in western North American forests as climate changes. Proc. Natl. Acad. Sci. USA, 14(18), 4582–4590, doi:10.1073/pnas.1617464114, 2017.

Smits, K. M., Cihan, A., Sakaki, T., and Illangasekare, T. H.: Evaporation from soils under thermal boundary conditions: Experimental and modeling investigation to compare equilibrium- and nonequilibrium-based approaches, Water Resour. Res., 47, W05540,
850   doi:10.1029/2010WR009533, 2011.

Smits, K. M., Kirby, E., Massman W. J., and Baggett, L, S.: Experimental and modeling study of forest fire effect on soil thermal conductivity, Pedosphere, 26, 462–473, doi:10.1016/S1002-0160(15)60057-1, 2016.

Stallman, R. W.: Steady one-dimensional fluid flow in a semi-infinite porous medium with sinusoidal surface temperature, J. Geophys. Res., 70, 2821–2827, doi:10.1029/JZ070i012p02821, 1965.

855   Stambaugh, M. C., Marschall, J. M., Abadir, E. R., Jones, B. C., Brose, P. H., Dey, D. C., and Guyette, R. P.: Wave of fire: an anthropogenic signal in historical fire regimes across central Pennsylvania, USA, Ecosphere, 9(5), e02222, doi:10.1002/ecs2.2222, 2018.

Tian, Z., Gao, W., Kool, D., Ren, T., Horton, R., and Heitman, J. L.: Approaches for estimating soil water retention curves at various bulk densities with the extended van Genuchten model, Water Resour. Res., 54, 5584–5601, doi:10.1029/2018WR022871, 2018.

Tian, Z., Lu, Y., Horton, R., and Ren, T.: A simplified de Vries-based model to estimate thermal conductivity of unfrozen and frozen soil,
860   European J. Soil Sci., 67, 564–572, doi:10.1111/ejss.12366, 2016.

Tong, B., Sauer, T. J., Gao, Z., Xiao, X., and Horton, R.: Improving soil heat flux accuracy with the Philip correction technique, J. Hydrometeor., 20, 1435–1448, doi:10.1175/JHM-D-18-0243.1, 2019.

Trautz, A. C., Smits, K. M., and Cihan, A.: Continuum-scale investigation of evaporation from bare soil under different boundary and initial conditions: An evaluation of nonequilibrium phase change, Water Resour. Res., 51, 7630–7648, doi:10.1002/2014WR016504, 2015.

865   Yoon, Y-S., Car, R., Srolovitz, D. J., and Scandolo, S.: Thermal conductivity of crystalline quartz from classical simulations, Physical Rev. B, 70, 012302, doi:10.1103/PhysRevB.70.012302, 2004.

Vallejo, V. R., and Alloza, J. A.: Postfire Ecosystem Restoration, in: Wildfire Hazards, Risks, and Disasters, edited by: Paton, D., Buergelt, P. T., McCaffrey, S., Tedim, F., and Shroder, J. F., Elsevier, Amsterdam, Netherlands, 229–246, doi:10.1016/B978-0-12-410434-1.00012-9, 2015.

870   van Genuchten, M. T.: A closed-form equation for predicting the hydraulic conductivity of unsaturated soils, Soil Sci. Soc. Am. J., 44, 892–898, doi:10.2136/sssaj1980.03615995004400050002x, 1980.
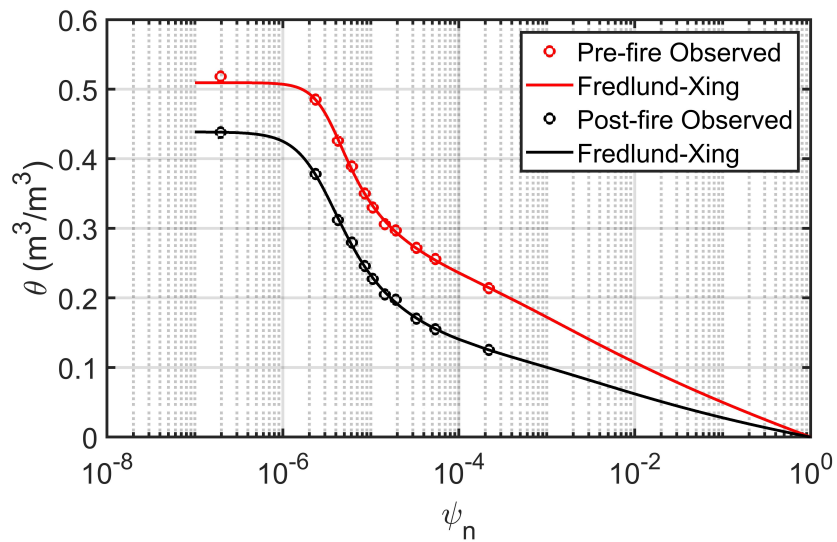
Figure 1. Pre- and post-burn water retention curves at the 2004 Manitou Experimental Forest burn site. Observations were fit with the Fredlund and Xing (1994) model. The only difference between these two curves is that the total or air-filled porosity is about 0.51 for the pre-burn (red) and it is about 0.45 for the post-burn (black).

Figure 2. Layout of the data system and slash pile of the Manitou Experimental Forest 26 April 2004 experimental burn a few minutes after ignition.
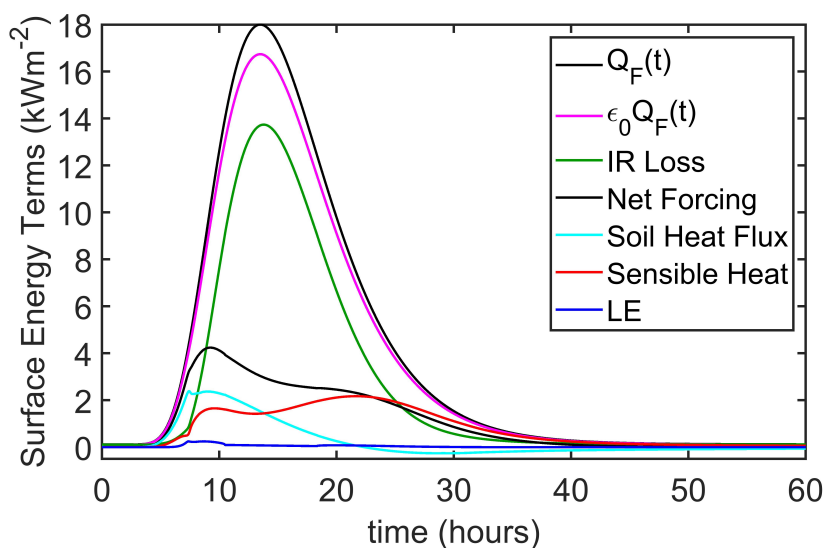
Figure 3. Soil surface energy balance components for the 26 April 2004 Manitou Experimental Forest burn resulting from the full surface energy balance model, Equation (16). The parameters for the forcing function, $Q_F(t)$ or Equation (15), are Q_{in} = 120 Wm^{-2}, Q_{Fmax} = 18 kWm^{-2}, t_m = 13.5 hrs and t_d = 35 hrs. The Net Forcing is defined as the difference between the radiative terms, i.e., $\epsilon_0(\theta_0)Q_F(t) - \epsilon_0(\theta_0)\sigma\left[T_{K0}^4 - \epsilon_a(\rho_{va})T_{Ka}^4\right]$, which from Equation (16) is equal to the sum of the three non-radiative terms: $\rho_a c_{pa} C_H \left[T_0 - T_a\right] + L_{v0}^* E_0 + G_0$. Figure 4 is an expanded version of the Net Forcing and these three energy components.
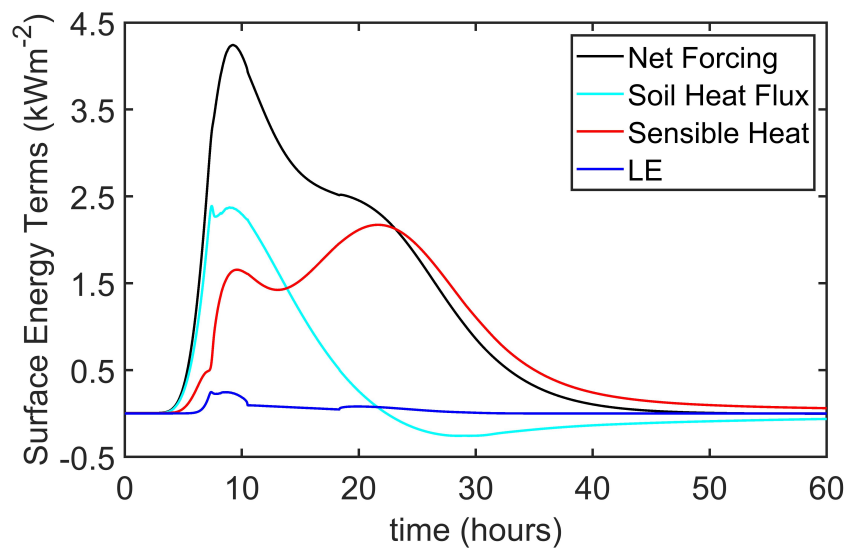
Figure 4. Re-plotted from Figure 3 to facilitate comparison with the surface energy terms as simulated with the simplified surface energy balance, Equation (18), and shown in Figure 5.
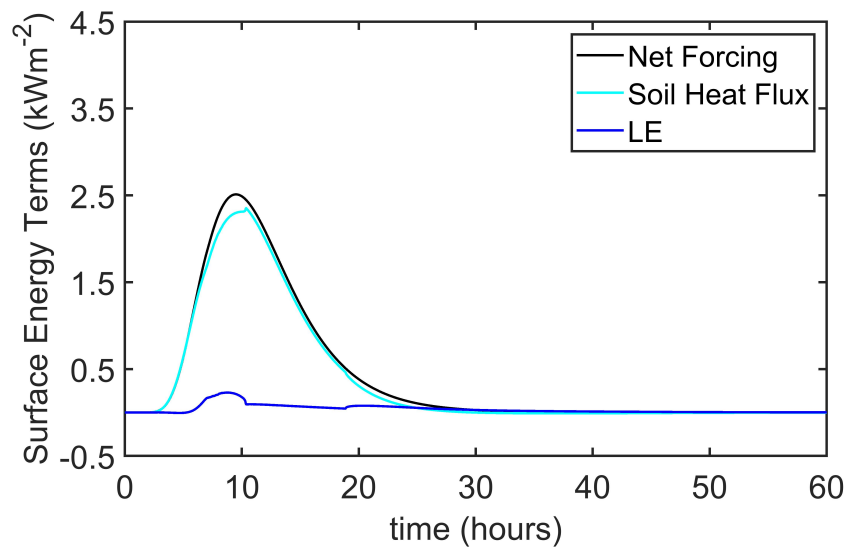
Figure 5. Soil surface energy balance components for the 26 April 2004 Manitou Experimental Forest burn resulting from the simplified surface energy balance model, Equation (18). The parameters for the forcing function, $Q_F(t)$ or Equation (15), are $Q_{in} = 0 \, \mathrm{Wm^{-2}}$, Q_{Fmax} = 2.7kWm^{-2}, t_m = 9.5 hrs and t_d = 27.5 hrs. Here the Net Forcing is the sum $L^*_{v0}E_0 + G_0$ because the surface sensible heat flux is not included as part the simplified surface energy balance.
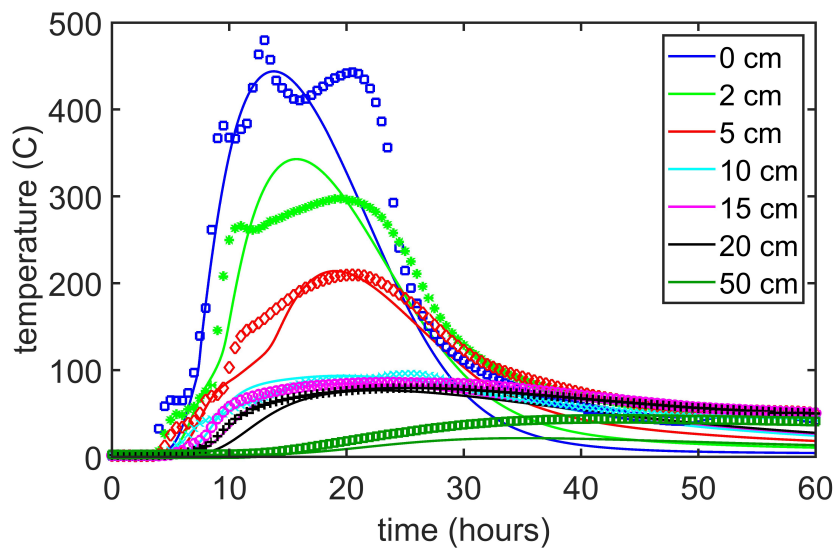
Figure 6. Soil temperatures during the 26 April 2004 Manitou Experimental Forest burn: observed data are denoted with symbols and modeling results (solid lines) are simulated with the full version of the soil surface energy balance, Equation (16).
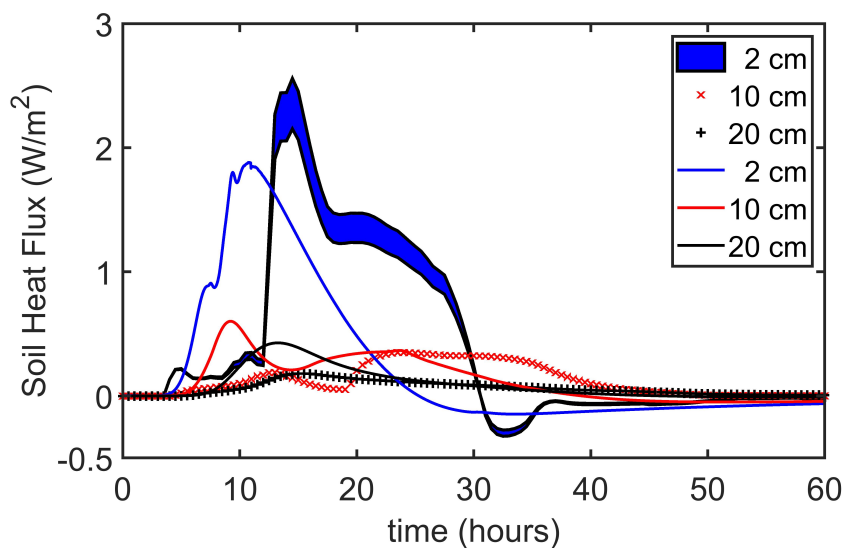
Figure 7. Soil heat flux during the 26 April 2004 Manitou Experimental Forest burn: modeled (solid lines) and observed (blue color-filled area and red and black symbols). The upper boundary of the (2 cm) blue color-filled region is the heat flux measured by the heat flux plate without the Philip correction (Philip , 1961). The lower boundary of this region is the measured heat flux after applying the Philip correction. The Philip correction is not shown for the two lower heat flux measurements because it made virtually no difference to these measurements.
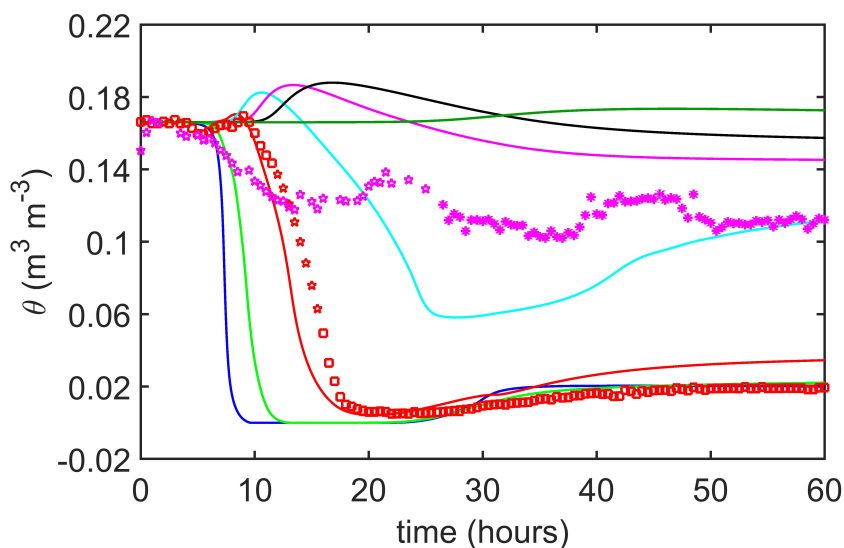
Figure 8. Volumetric soil moisture, after temperature correction to the TDR probe (Massman et al. , 2010a, Appendix A), during the 26 April 2004 Manitou Experimental Forest burn: modeled (solid lines) and observed (symbols). The color coding for depth is the same as that in Figure 6, but observations of soil moisture are taken only at two depths 5 cm (red) and 15 cm (magenta). The red stars are interpolated values and appear to be fairly trustworthy. The magenta stars are less trustworthy because the performance of the 15 cm TDR during the early part of the burn was not completely satisfactory.
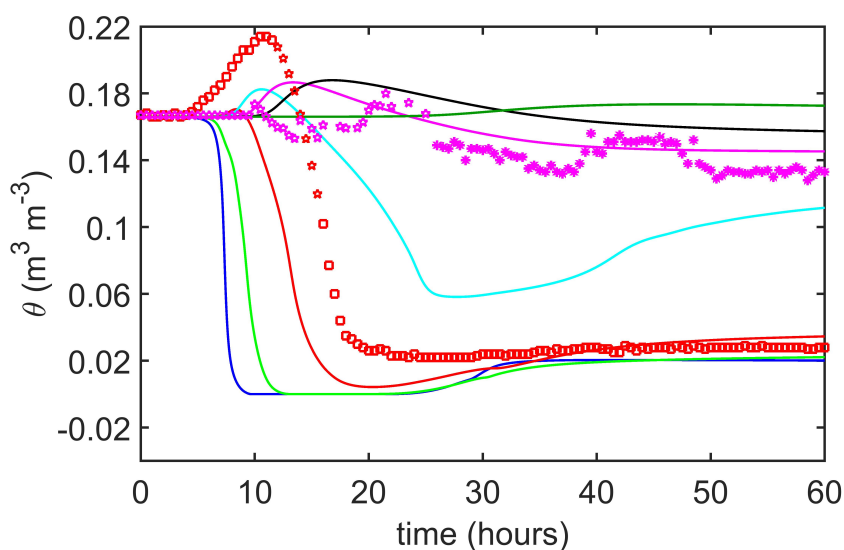
Figure 9. Volumetric soil moisture, without temperature correction to the TDR (Massman et al. , 2010a, Appendix A) during the 26 April 2004 Manitou Experimental Forest burn: modeled (solid lines) and observed (symbols). The color coding for depth is the same as that in Figure 6, but observations of soil moisture are taken only at two depths 5 cm (red) and 15 cm (magenta). The red stars are interpolated values and appear to be fairly trustworthy. The magenta stars are less trustworthy because the performance of the 15 cm TDR during the early part of the burn was not completely satisfactory.
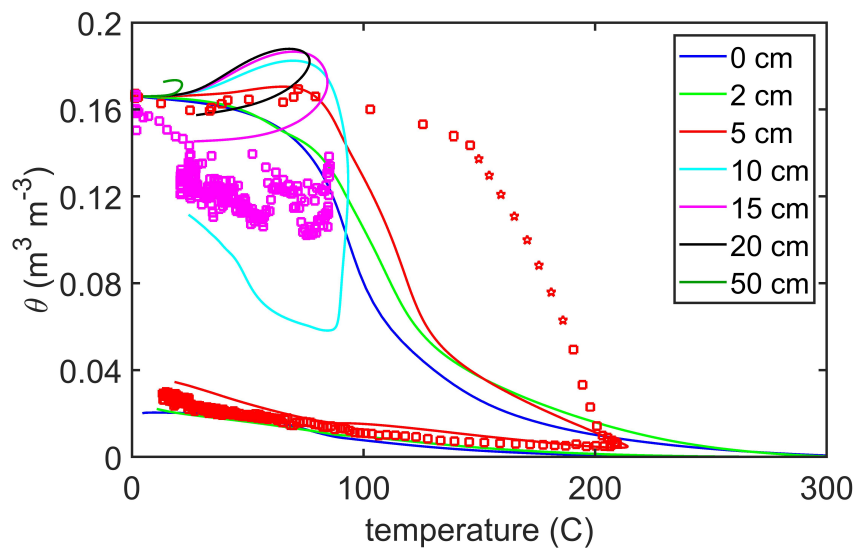
Figure 10. Modeled and observed $\theta - T$ trajectory. Observed data are denoted with symbols and modeling results are solid lines. The observed volumetric soil moisture has been temperature corrected.
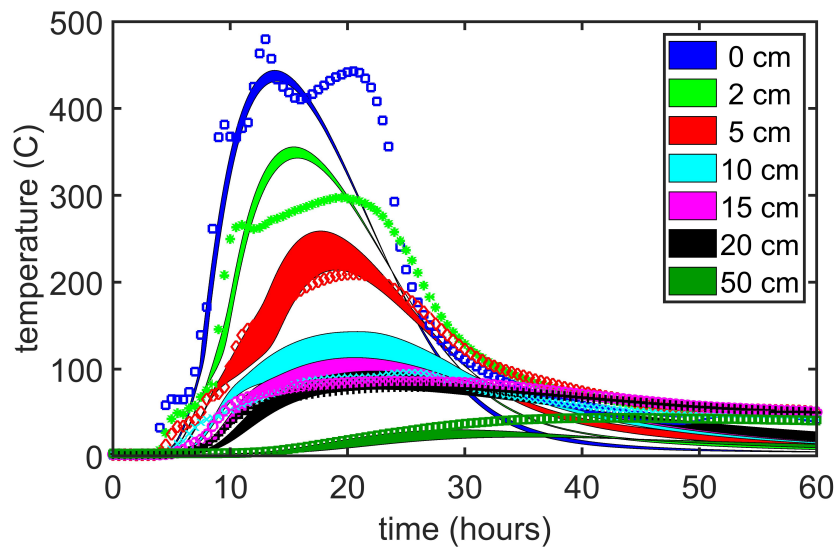
Figure 11. Potential impacts of dynamic feedbacks on the soil temperatures during the 26 April 2004 Manitou Experimental Forest burn. Observed data are denoted with symbols and modeling results are solid filled areas. The lower boundary of the solid filled areas corresponds to the base case simulation and the upper boundary to the feedback simulation.
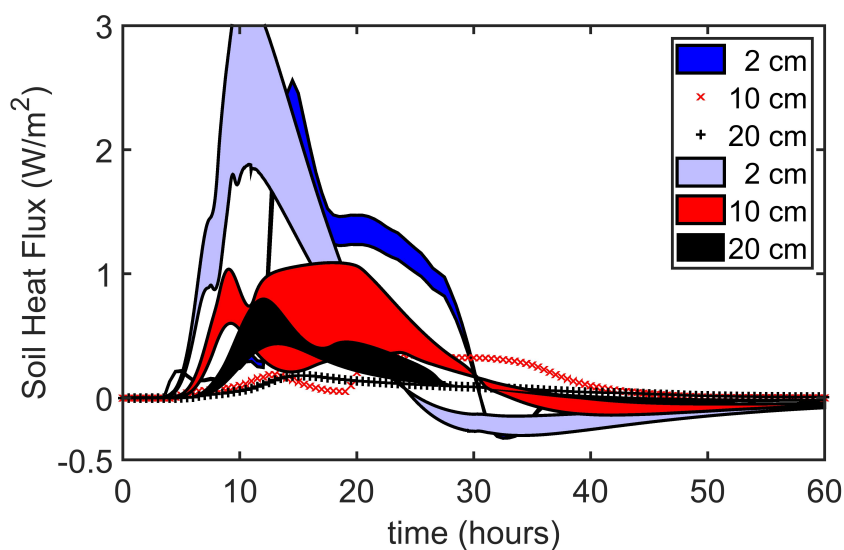
Figure 12. Potential impacts of dynamic feedbacks on the soil heat flux during the 26 April 2004 Manitou Experimental Forest burn. The observed data are the (2 cm) darker blue color-filled area and red and black symbols. The upper boundary of the observed heat flux includes the Philip correction; wheras the lower boundary of this region is the measured heat flux after applying the Philip correction. The Philip correction is not shown for the two lower heat flux measurements because it made virtually no difference to these measurements. The upper boundary of the light-blue, red and black color-filled areas corresponds to the feedback simulation and the lower boundary to the base case simulation.
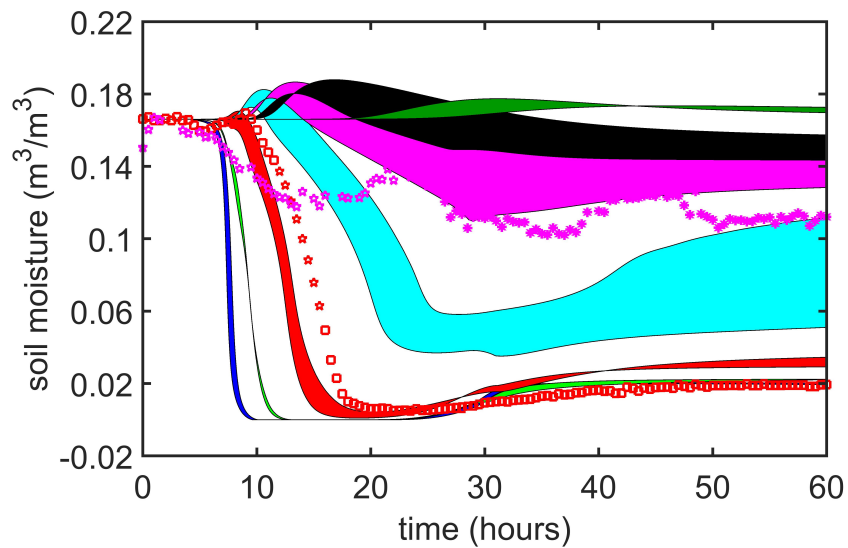
Figure 13. Potential impacts of dynamic feedbacks on the volumetric soil moisture during the 26 April 2004 Manitou Experimental Forest burn. Observed data, which has been temperature corrected, are denoted with symbols and modeling results are solid filled areas. The upper boundary of the solid filled areas corresponds to the base case simulation. The lower boundary to the feedback simulation.